Published online 8 December 2022 *Nucleic Acids Research, 2022, Vol. 50, No. 21* ***12291–12308***
https://doi.org/10.1093/nar/gkac1153

PARG and BRCA1–BARD1 cooperative function regulates DNA repair pathway choice during gametogenesis

Shalini Trivedi, Jitka Blazícková and Nicola Silva *

Department of Biology, Faculty of Medicine, Masaryk University, Kamenice 5, 62500 Brno, Czech Republic

Received June 23, 2022; Revised November 09, 2022; Editorial Decision November 14, 2022; Accepted November 18, 2022

ABSTRACT

Meiotic chromosome segregation relies on programmed DNA double-strand break induction. These are in turn repaired by homologous recombination, generating physical attachments between the parental chromosomes called crossovers. A subset of breaks yields recombinant outcomes, while crossover-independent mechanisms repair the majority of lesions. The balance between different repair pathways is crucial to ensure genome integrity. We show that *Caenorhabditis elegans* BRC-1/BRCA1-BRD-1/BARD1 and PARG-1/PARG form a complex *in vivo*, essential for accurate DNA repair in the germline. Simultaneous depletion of BRC-1 and PARG-1 causes synthetic lethality due to reduced crossover formation and impaired break repair, evidenced by hindered RPA-1 removal and presence of aberrant chromatin bodies in diakinesis nuclei, whose formation depends on *spo-11* function. These factors undergo a similar yet independent loading in developing oocytes, consistent with operating in different pathways. Abrogation of KU- or Theta-mediated end joining elicits opposite effects in *brc-1; parg-1* doubles, suggesting a profound impact in influencing DNA repair pathway choice by BRC-1-PARG-1. Importantly, lack of PARG-1 catalytic activity suppresses untimely accumulation of RAD-51 foci in *brc-1* mutants but is only partially required for fertility. Our data show that BRC-1/BRD-1–PARG-1 joint function is essential for genome integrity in meiotic cells by regulating multiple DNA repair pathways.

INTRODUCTION

Genome integrity is constantly challenged by exogenous sources (e.g. chemicals, radiations), however genotoxic insults can also arise within the cellular environment and affect DNA stability, such as upon oxidative stress or errors during replication and transcription. Severing of both DNA strands (double-strand breaks, DSBs) is one of the most toxic types of DNA damage and if not promptly resolved, it can result in cell death or chromosome aberrations (deletions, translocations), often linked to cellular transformation. Importantly, alterations of the genetic material occurring in the germline can give rise to inheritable mutations, leading to predisposition to cancer and sterility.

During meiosis, DNA replication is followed by two consecutive rounds of cell division, producing haploid gametes that will reconstitute ploidy upon fertilization. Meiotic progression is characterized by many unique features, all harmoniously coordinated to ensure equal partitioning of the genetic material into the daughter cells. The paternal and maternal chromosomes (homologous chromosomes) undergo active motion at meiosis onset until homology is satisfied (homologous pairing), then their association is stabilized by the synaptonemal complex (SC), in whose context homologous recombination can take place and ultimately produce chiasmata (1,2). These are the cytological manifestation of a crossover (CO), whereby a physical exchange of DNA molecules between the homologs has been achieved. COs are crucial for the correct segregation of the homologous chromosomes during the first meiotic division, as they act as a physical tether that provides the tension required when the pulling forces exerted by the spindle promote the migration of each homolog to the opposite poles of the dividing cell. Failure in CO establishment results in achiasmatic chromosomes that undergo random segregation in the daughter cells, thus causing formation of aneuploid gametes.

COs are formed via homologous recombination (HR) upon the deliberate induction of DSBs triggered by the topoisomerase-like Spo11 (3), which produces many cuts onto the DNA in order to ensure that at least one for each chromosome pair will be converted into a chiasma. Resolution of the remaining DSBs is channelled into CO-independent, homology-mediated DNA repair pathways (non-CO, NCO) thus restoring genome integrity. Meiotic DSB repair must be strongly regulated in order to preserve fidelity of the genetic information and therefore it relies on

*To whom correspondence should be addressed. Tel: +420 549 49 8033; Email: silva@med.muni.cz

conservative DNA repair mechanisms. Error-prone pathways such as canonical or alternative end joining are normally shut down during meiotic progression, however they can be activated under dysfunctional homologous recombination (4–7).

The tumour suppressor E3 ubiquitin ligase complex BRCA1–BARD1 has been shown to play crucial roles during HR in mitotic cells and in more recent years its roles during meiosis have become increasingly more investigated (8). In *Caenorhabditis elegans*, BRC-1/BRCA1 and BRD-1/BARD1 are essential to promote inter-sister repair pathway of meiotic DSBs, to stabilize the loading of the recombinase RAD-51/RecA during meiotic progression and recent work has highlighted roles in differentially regulating the recombination rate in oocytes and sperms (8–10). We have previously shown that the *C. elegans* ortholog of mammalian poly(ADP-ribose) glycohydrolase *PARG*, *parg-1*, plays crucial roles in ensuring efficient formation of meiotic DSBs as well as promoting their repair via HR during meiosis (11). However, the pathway(s) intersected by PARG-1 function during DSB repair in the germ cells have remained largely unknown. Here, we show that PARG-1 forms a complex with BRC-1 and BRD-1 *in vivo* and simultaneous depletion of these factors leads to a severe impairment of fertility and weakening of CO homeostasis, most notably on the X chromosome. SPO-11-dependent DSBs are formed in *brc-1; parg-1* double mutants however their processing is severely compromised, as indicated by accumulation of RAD-51 foci at late pachytene stage and impaired RPA-1 removal. This culminates in the generation of morphologically aberrant chromosomes in the diakinesis nuclei whose formation requires SPO-11 function.

We found that abrogation of canonical or alternative non-homologous end joining (cNHEJ and aNHEJ, respectively) causes opposite phenotypes in the *brc-1; parg-1* doubles, unveiling an essential function for aNHEJ in preserving fertility levels in both *brc-1* and *brc-1; parg-1* mutants. Furthermore, PARG-1 catalytic activity is responsible for delayed RAD-51 loading in *brc-1* mutants but only partially required to prevent synthetic lethality, indicating that loading of PARG-1 along the chromosomes holds more essential roles in meiotic cells than its enzymatic activity. Our data show that BRC-1-BRD-1 and PARG-1 establish a functional hub that acts as a switch in DNA repair pathway choice and therefore their combined function is essential to maintain genome integrity during gametogenesis.

MATERIALS AND METHODS

Genetics and screenings

C. elegans N2 was used as wild type control. Worms were grown on NGM plates according to standard procedures (12) and maintained at 20°C for all the experiments. A full list of the strains used in this study is provided as Supplementary Table S1. Viability and male progeny assessment was performed on single worms of the indicated genotypes, that were transferred onto a fresh plate every 24h. Dead eggs were scored 24h after the mother had been removed and male progeny was counted three days later. For assessment of post-embryonic development, the number of worms in each stage (L1, L2, L3, L4 and adults) was counted 72h after the mother had been removed and quantified as percentage over the total number of hatched eggs.

Immunostaining and image acquisition

Samples were dissected and fixed as in (9) without modifications, except that incubation of primary antibodies was carried out overnight at room temperature. Primary antibodies used in cytological analyses were: mouse anti-GFP 1:500 (Roche, #11814460001), mouse anti-HA 1:600 (Biolegend, #901513), rabbit anti-HA pre-absorbed against untagged animals 1:100 (Sigma, #H6908), rabbit anti-OLLAS tag pre-absorbed against untagged animals 1:500 (Genscript, #A01658), mouse anti-FLAG pre-absorbed against untagged animals 1:500 (Sigma, #F1804), rabbit anti-SYP-1 (11) (1:1000), chicken anti-SYP-1 1:400 (15), rabbit anti-BRD-1 pre-absorbed against *brd-1(dw1)* null worms, 1:400 (13), rabbit anti-RAD-51 1:3000 (14), chicken anti-RAD-51 1:1000 (15), guinea pig anti-HTP-3 1:700 (Y. Kim lab), rabbit anti-HIM-8 1:500 (Novus Biologicals, # 41980002). All Alexa Fluor 488 or 647 conjugated secondary antibodies were used at 1:500, while Alexa Fluor conjugated to 594 was used at 1:700 (ThermoFisher).

Slides were imaged with an upright Zeiss AxioImager.Z2 with a 100x objective, equipped with a Monochromatic camera Hamamatsu ORCA Fusion (sCMOS sensor, 2304 × 2304 pixels, 6.5 × 6.5 μm size). Z-stacks were set at 0.24 μm thickness and images were deconvolved using Zen Blue with the 'constrained iteration' method set at maximum strength. Images were further processed in Photoshop, where some false colouring was applied (red and green channels were swapped or the hue was changed for visual purposes). For images in Figure 3C and Supplementary Figure S5, samples were acquired with a Delta Vision microscope with a 100x objective, equipped with an Evolve 512 EMCCD Camera and deconvolved with Softworx.

For quantification of RAD-51 and synapsis, at least three germ lines of the indicated genotypes were used, which were divided into seven equal regions from the mitotic tip to the late pachytene stage. Zone 1 and Zone 2 correspond to the pre-meiotic region, Zone 3 spans the transition zone, Zone 4 overlaps with early pachytene, Zone 5 includes early-mid pachytene stage, Zone 6 corresponds to mid-late pachytene and Zone 7 to late pachytene/diplotene entry. The number of RAD-51 foci was counted in each nucleus and the average was plotted in the charts. The nuclei in late pachytene stage displaying obvious apoptotic features such as chromatin over condensation or reduced nucleus diameter (pyknotic cells) were discarded from the counts.

For SC assessment, nuclei were considered synapsed only if HTP-3 signal fully overlapped with SYP-1. The number of the nuclei quantified in each genotype are reported in Supplementary Table S2.

For quantification of OLLAS::RPA-1 foci, nuclei from diplotene entry to -1 diakinesis were scored and their number is reported in Supplementary Table S3.

For OLLAS::COSA-1 quantification, only nuclei within the last seven rows of cells before diplotene entry were scored and their number is reported in Supplementary Table S4.

For 3xHA::DSB-1 quantification, at least three gonads for each genotype were used and assessment of DSB-1 staining was performed by counting the number of positive cell rows for DSB-1 (a cell row was considered 'positive' only when at least 50% of the nuclei displayed DSB-1 staining) and then normalized over the total number of cell rows, as similarly done for pSUN-1^{S8} or PLK-2 staining (16,17).

Diakinesis chromosome analyses

Worms of the indicated genotypes were selected as L4s and dissected at the indicated times. Animals were dissected and fixed as for regular immunostaining protocol. Once the slides were removed from methanol, they were washed three times in 1× PBS containing 0.1% Tween and 60 μl of a 2μg/ml solution of 4′,6-diamidino-2-phenylindole (DAPI) in water was applied to each slide and left for 1 min in the dark. Samples were washed for 20 min in the dark in 1× PBST and mounted with Vectashield.

For the analysis of the DAPI bodies, only the −1 and −2 diakinesis nuclei were included in the counts. The number of the nuclei quantified in each genotype are reported in Supplementary Table S4.

Immmunoprecipitation and western blot

Immunoprecipitations were performed by employing nuclear protein extracts containing both nuclear soluble and chromatin-bound fractions produced as in (16) without modifications, except that Complete protease inhibitor (Roche) at 1× final concentration was supplemented to all buffers used for the protein fractionation in addition to the protease inhibitor solution provided with the protein extraction kit (Qproteome nuclear protein kit, Qiagen). Chromatin-bound fraction was produced upon Benzonase digestion (25 U for 100 μl of nuclear extract) for 1 h at 4°C. 1 mg of protein extracts was incubated with agarose GFP traps (Chromotek, #GTA-20) pre-equilibrated with Buffer D (20 mM HEPES pH 7.9, 150 mM KCl, 20% glycerol, 0.2 mM EDTA, 0.2% Triton X-100 and complete Roche inhibitor) and carried out on a rotating wheel over night at 4°C. 100 μg of protein extracts (10% of the amount used for the IPs) was run for the inputs. The following day, the samples were spun down at 7500 rpm for 2 min and supernatants were discarded. Beads were extensively washed with Buffer D and then resuspended in 40 μl of 2× Laemmli buffer before being boiled for 10 min. Eluates were separated from the beads by centrifugation at maximum speed for 2 min and loaded onto a precast 4–20% acrylamide gel (Bio-Rad), run in Tris-Glycine SDS buffer, and transferred onto a nitrocellulose membrane at 100 V for 90 min at 4°C. Blots were blocked in 5% milk in 1× TBS containing 0.1% Tween for 1 h at room temperature and primary antibodies were incubated overnight at 4°C. All secondary antibodies were diluted in 5% milk in 1× TBS containing 0.1% Tween and allowed to incubate for 2 h at room temperature. Primary antibodies used for western blot were: mouse anti-HA 1:1000 (Cell Signaling, #2367), mouse anti-PARG-1 1:500 (11), chicken anti-GFP 1:5000 (Abcam, #ab13970), mouse anti-actin 1:1000 (Santa Cruz, #sc-8432), mouse anti-tubulin 1:2000 (Sigma, #T5168).

Fluorescence *In Situ* Hybridization

FISH was performed as in (16). Briefly, synchronized young adults (24 h post-L4) were dissected in 1× EGG buffer (118 mM NaCl, 48 mM KCl, 2 mM $CaCl_2$, 2 mM $MgCl_2$, 25 mM HEPES, pH 7.3) containing 0.1% tween and fixed with an equal amount of 7.4% of formaldehyde for 2 min at room temperature. Coverslips were freeze-cracked in liquid nitrogen and slides were placed in methanol at –20°C for at least 5 min. Slides were placed in 50% methanol in 1× SSC for 1 minute at room temperature and then three washes in 2× SSC with 0.1% tween for 5 min each were carried out at room temperature. Samples were placed in 70%, 90% and 100% ethanol at room temperature for 3 min each, after which they were air dried. Probes were applied in FISH-mix (10% dextran sulphate, 50% formamide, 2× SSC with 0.1% tween) and hybridization was performed in a slide thermomixer at 93°C for 3 min, 72°C for 2 min and 37°C overnight. The following day, a 37°C prewarmed solution of 50% formamide in 2× SCC with 0.1% tween was used to carry two post-hybridization washes of 30 min each at 37°C and then slides were further washed in 2× SCC with 0.1% tween three times for 10 min each at room temperature. Samples were blocked for 30 min in a solution of 1% BSA in 2× SSC with 0.1% tween at room temperature and then rhodamine-conjugated anti-digoxigenin (Roche, #11207750910) or FITC-conjugated anti-biotin (AbCam, #ab6650) used at a 1:200 and 1:500 dilution respectively, were left to incubate for 3 h at room temperature in the dark. Slides were washed three times for 10 min each in 2× SSC with 0.1% tween in the dark and 60 μl of a 2 μg/ml solution of DAPI was applied for 2 min. Samples were further washed for 20 min in 2× SSC with 0.1% tween in the dark and then sealed with Vectashield.

The T17A3 cosmid was used to generate the probe recognizing the left end of chromosome III. The cosmid clone was grown in bacteria and purified with the miniprep kit from Qiagen according to the manufacturer instructions. The probe annealing to the right end of chromosome V was produced by amplifying the endogenous 5s rDNA locus by PCR with primers 5′-TACTTGGATCGGAGACGGCC-3′ and 5′- CTAACTGGACTCAACGTTGC-3′. Multiple PCR reactions were pooled and column-purified according to manufacturer instructions (Macherey-Nagel). 1 μg of DNA was labelled by nick-translation with digoxigenin for chromosome III (Roche, 11745816910) or biotin for chromosome V (Roche 11745824910) according to manufacturer instructions and 1.5 μl of each labelled probe was applied per slide.

CRISPR/Cas9 genome editing

All transgenic lines were generated by CRISPR as in Paix *et al.* (18). Briefly, synthetic Ultramers carrying the desired changes were purchased (IDT) and included in a mix containing tracer RNA and Cas9 protein, the sgRNAs targeting the locus of interest and the *dpy-10* gene (used as a co-editing marker). Tubes were incubated at 37°C for 15 min, spun down at 14 000 rpm for 2 min and then directly used for injections. WT worms were microinjected (P0) and F1 L4 animals with a *roller* phenotype were individually picked

and then used for PCR analysis to identify the heterozygous edits. Non-rollers worms from F2 progeny were individually picked, and PCR were performed to identify the homozygous animals. All strains generated by CRISPR were outcrossed to N2 wild type animals at least twice before use.

RESULTS

PARG-1 interacts with BRC-1 and BRD-1 *in vivo*

We have recently shown that PARG-1/PARG exerts important roles during induction and repair of meiotic DSBs in *C. elegans*. PARG-1 removal both exacerbates CO defects in mutant backgrounds with reduced DSBs and also partially alleviates chromosome abnormalities observed in diakinesis nuclei of mutants with impaired HR-mediated repair (11). These results indicate that PARG-1 can, either directly or indirectly, not only stimulate DSB formation but also influence DNA repair pathway choice.

In order to shed light on the repair pathways influenced by *parg-1* function, we decided to investigate its possible link(s) to other factors known to regulate meiotic DSB repair. In particular, we sought to assess whether *parg-1* establishes functional interactions with the E3 ubiquitin ligase heterodimer BRC-1-BRD-1 (9,11). BRC-1 and BRD-1 operate in an obligate heterodimeric complex both in mammals and nematodes (9,19). We first chose to determine whether there are physical interactions between these proteins by taking advantage of functionally tagged lines for these factors that we had previously characterized (9,11). Therefore, we constructed the *brc-1::HA; parg-1::GFP* and *brd-1::HA; parg-1::GFP* strains to perform co-immunoprecipitation experiments.

We observed specific co-immunoprecipitation of both BRC-1 and BRD-1 with PARG-1::GFP (Figure 1A, Supplementary Figure S1A), indicating that these proteins associate *in vivo*. Detection of BRC-1::HA and BRD-1::HA appeared as multiple bands, which may indicate alternative isoforms or cleavage and/or partial degradation products generated with this protein extraction/fractionation method (16).

Given their physical interaction, we next addressed whether these factors influenced each other´s expression or whether they were interdependent for loading. Immunofluorescence analysis of PARG-1::GFP and BRC-1::HA/BRD-1::HA (or endogenous BRD-1) showed that these factors localize similarly during meiotic Prophase I, gradually switching from a diffuse nuclear localization in the early stages of meiotic progression to enrichment along the synapsed chromosomes (9,11) (Figure 1B, Supplementary Figure S1B-C). Our cytological data indicated that PARG-1::GFP was normally loaded in *brc-1(ddr41)* null mutants (Figure 1C) and conversely, that BRC-1::HA (Figure 1D) or BRD-1 recruitment (Figure 1E) was not altered in absence of *parg-1*. We extended this analysis by performing Western blot on total worm extracts, which revealed that the stability of BRC-1::HA and BRD-1::HA is not affected in the *parg-1* mutant and that PARG-1 levels in *brc-1* and *brd-1* null mutants were similar to wild type controls (Figure 1F). Thus, we conclude that while PARG-1 is associated with BRC-1-BRD-1 *in vivo* and displays a similar localization in developing oocytes, these proteins do not undergo interdependent chromosome loading.

Contemporaneous removal of parg-1 and brc-1 impairs fertility levels

Both *parg-1* and *brc-1* null mutants show nearly normal hatching rates under physiological growth conditions consistently with prior observation that they are fully proficient in homologous pairing, installation and maintenance of the synaptonemal complex, and crossover establishment (9,11,20). Based on their *in vivo* association, we wondered whether removal of both *brc-1* and *parg-1* would elicit synthetic effects during gametogenesis. We generated the *brc-1; parg-1* double mutant strain and observed high levels of embryonic lethality (Figure 2A) and segregation of male progeny amongst the survivors (Figure 2B), consistent with defects in chromosome segregation of autosomes and the chromosome X, respectively (21). While the global embryonic lethality (calculated as the total number of unhatched eggs/total laid eggs) neared 60%, we noticed that the number of dead embryos was not distributed evenly during the laying period, but rather showed a steady increase culminating in almost complete lethality at the last day of deposition (day 3, 72h), suggesting detrimental effects of age on fertility in the *brc-1; parg-1* background.

Impairment of different steps during meiotic progression can result in aberrant chromosome morphology and/or number in the diakinesis nuclei. Chromosome composition at this last stage of meiotic prophase I can therefore be used as a read-out of the events that occurred earlier (22). Absent or reduced levels of meiotic DSBs leads to the formation of achiasmatic chromosomes with a regular, ovoid shape (univalents) (23–26). Univalents are similarly formed upon (i) deficient conversion of the recombination intermediates into post-recombination products (e.g. *msh-4/5* or *cosa-1/CNTD1* mutants) (27–29) or (ii) by lack of/incomplete synapsis (30,31). On the other hand, dysfunctional DSB repair and deficient end-resection can cause reduced numbers of chiasmata which—in most instances—is coupled with abnormal chromosome morphology, including unstructured or fragmented DAPI bodies in the diakinesis nuclei (7,32–34). Therefore, given the high levels of embryonic lethality observed in the *brc-1; parg-1* double mutants, we sought to determine if diakinesis nuclei were affected. This analysis revealed that lack of both *brc-1* and *parg-1* resulted in both aberrant chromosome morphologies and changes in the number of DAPI bodies, with nuclei containing unstructured chromatin masses, univalent, and/or fragments as well as seemingly normal bivalents (Figure 2C, D). Consistent with age-dependent worsening of viability in the *brc-1; parg-1* double mutants, we observed that the frequency of diakinesis nuclei bearing abnormal chromosome figures was higher in older animals (Supplementary Figure S1D). Removal of *spo-11* suppressed the formation of morphologically aberrant DAPI-bodies in the diakinesis nuclei of *brc-1; parg-1* doubles (Figure 2C, D) and led to formation of normally-shaped univalents. This result indicates that meiotic DSBs are formed but not properly repaired in the *brc-1; parg-1* double mutants due to either defective DNA repair or pathways usage or as a consequence of perturbed end resection.

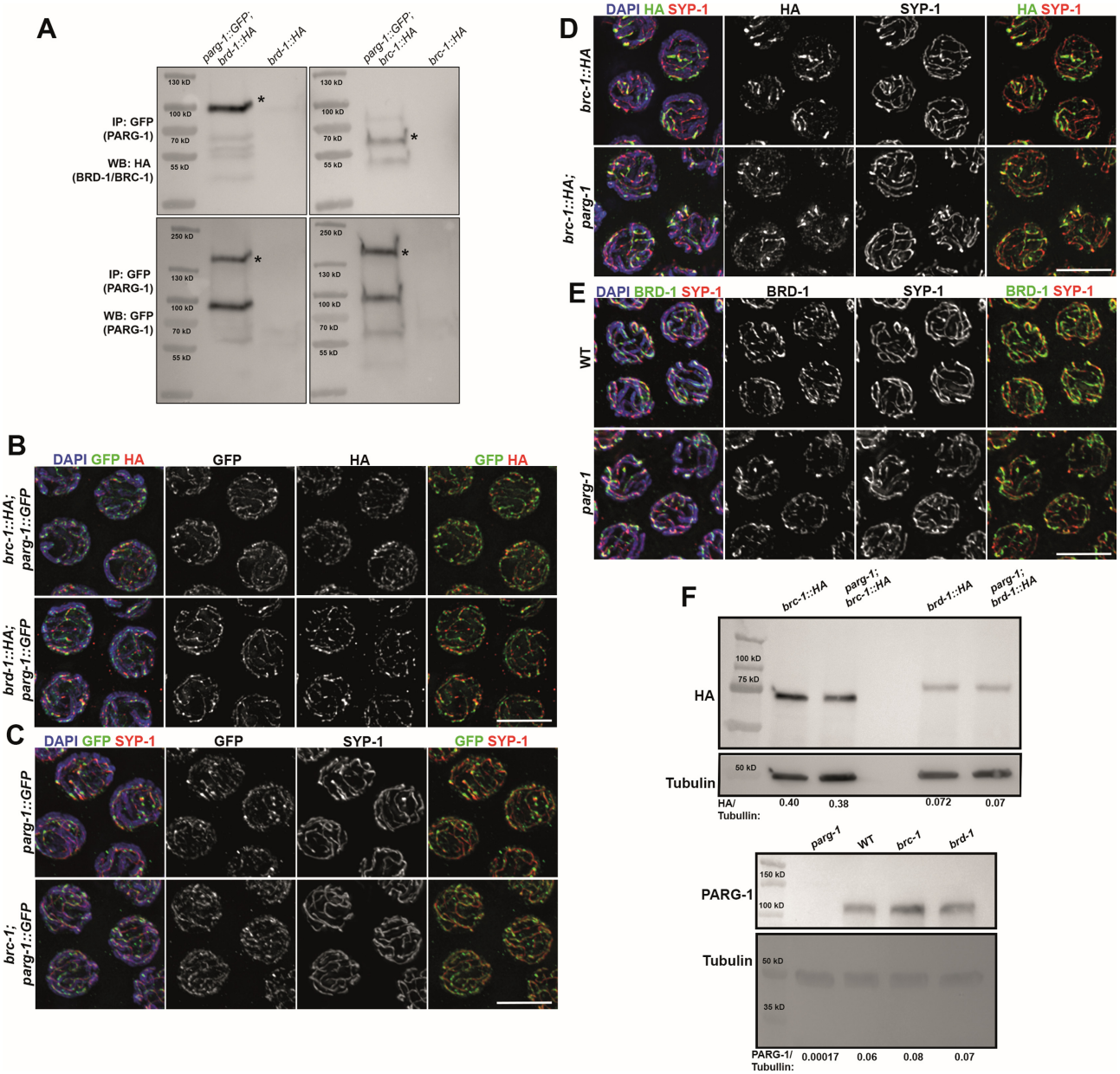

Figure 1. PARG-1 and BRC-1/BRD-1 interact *in vivo*. (**A**) Immunoprecipitation of PARG-1::GFP in *brc-1::HA* and *brd-1::HA* strains reveals physical interaction. Asterisks indicate the putative main form of the proteins of interest. (**B**) Mid-pachytene nuclei stained for HA/GFP showing that BRC-1, BRD-1 and PARG-1 display similar localization along synapsed chromosomes. Scale bar 5 μm. (**C**) Mid-late pachytene nuclei showing that PARG-1::GFP loading does not require BRC-1. Scale bar 5 μm. (**D**) Mid-late pachytene nuclei showing that recruitment of BRC-1::HA and (**E**) BRD-1 (detected with an antibody directed against endogenous BRD-1) along the chromosomes is independent of *parg-1* function. Scale bar 5 μm. (**F**) Western blot on total protein extracts showing that absence of *parg-1* does not alter BRC-1 and BRD-1 expression/stability (top), and PARG-1 protein levels are unchanged in *brc-1* and *brd-1* mutants (bottom). Tubulin was used as loading control.

PARG-1–BRC-1 joint function regulates the processing of recombination intermediates

Given that the analysis of the diakinesis nuclei in *brc-1; parg-1* doubles revealed a highly variable, *spo-11*-dependent phenotype, we then wanted to investigate both the formation and repair dynamics of recombination intermediates by analysing RAD-51 recruitment to DNA. RAD-51 is the main recombinase in *C. elegans* and its loading follows a reproducible pattern in wild-type animals. Few foci appear at meiotic entry (leptotene/zygotene), they peak at the early-mid pachytene transition, and disengage from chromatin at mid-late pachytene stage, indicating completion of repair (30,35).

Prior studies showed that *brc-1* null mutant hermaphrodites display roughly normal RAD-51 loading in early pachytene but accumulate excessive foci in late pachytene (9,10,20). By contrast, *parg-1* mutants have altered early dynamics of RAD-51 staining compared to wild type with slower accumulation of RAD-51 foci

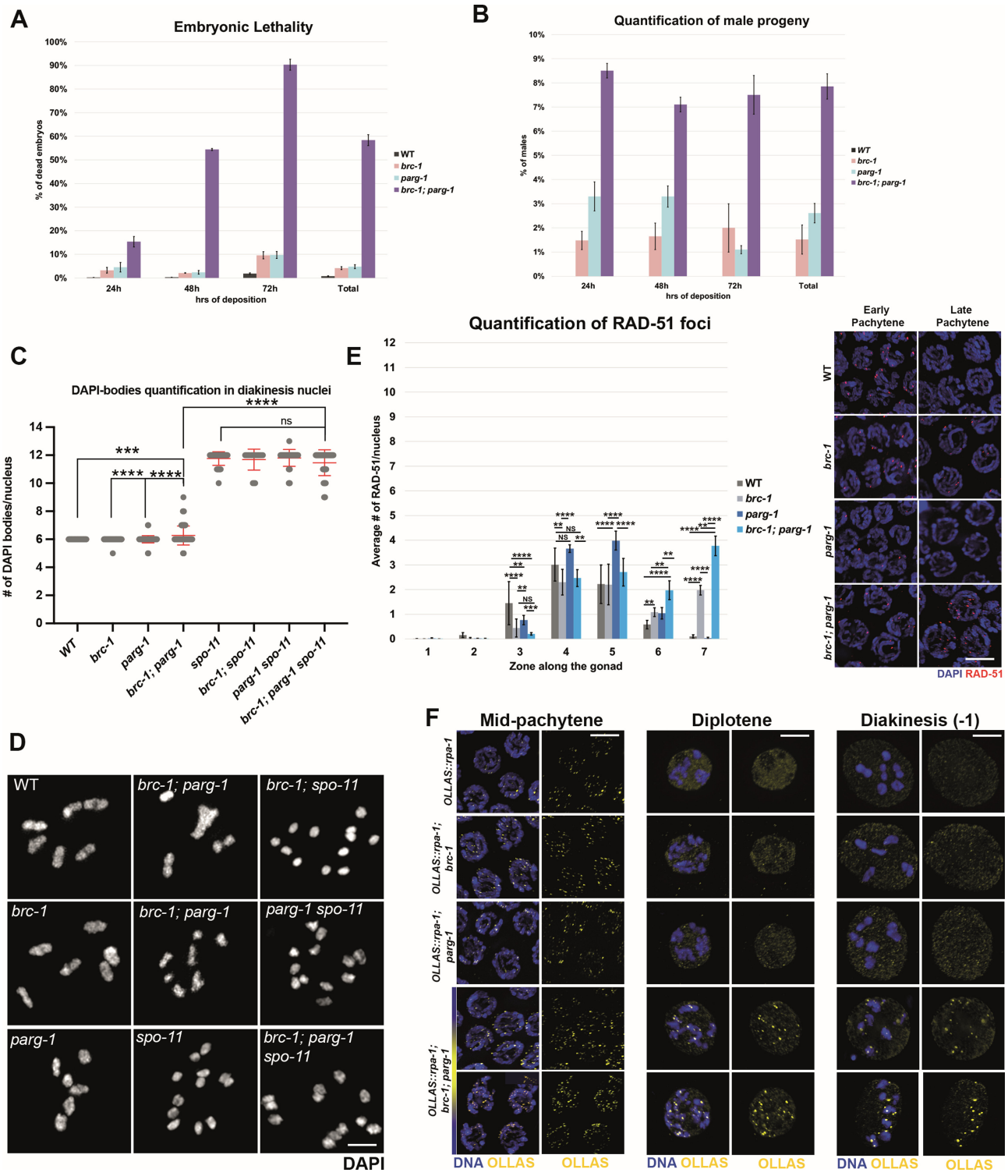

Figure 2. Lack of *brc-1-parg-1* causes severe genome instability. (**A**) Assessment of embryonic lethality in the indicated genotypes. The columns in the 'total' data point depict sum of all dead embryos/laid eggs over the three-day deposition window. Bars report mean with SEM. (**B**) Assessment of male progeny in the indicated genotype performed as in (A). (**C**) Quantification of DAPI-bodies and (**D**) representative images of diakinesis nuclei in the indicated strains. Bars indicate mean ± SD, asterisks denote statistically significant differences (***$P = 0.0003$, ****$P < 0.0001$, ^{ns}non-significant) as calculated by *t* test. Scale bar 5 μm. (**E**) Left: quantification of RAD-51 foci formation in the indicated genotypes. X-axis indicates zone along the gonad (see Methods), Y-axis shows average number of RAD-51 foci/nucleus. Bars represent mean with ± SEM and asterisks indicate statistically significant differences (Zone 3:**$P = 0.0036$, ****$P < 0.0001$, ^{ns}non-significant; Zone 4:**$P = 0.007$, ****$P < 0.0001$, ^{ns}non-significant; Zone 5:****$P < 0.0001$; Zone 6:**$P = 0.002$, ****$P < 0.0001$; Zone 7:**$P = 0.0059$, ****$P < 0.0001$) as calculated by Kruskal–Wallis test. Right: representative images of nuclei at the indicated stages and genotypes, stained for RAD-51 and DAPI. Scale bar 5 μm. (**F**) Nuclei of the indicated genotypes and stages, stained for OLLAS::RPA-1 and DAPI. Scale bar 5 μm.

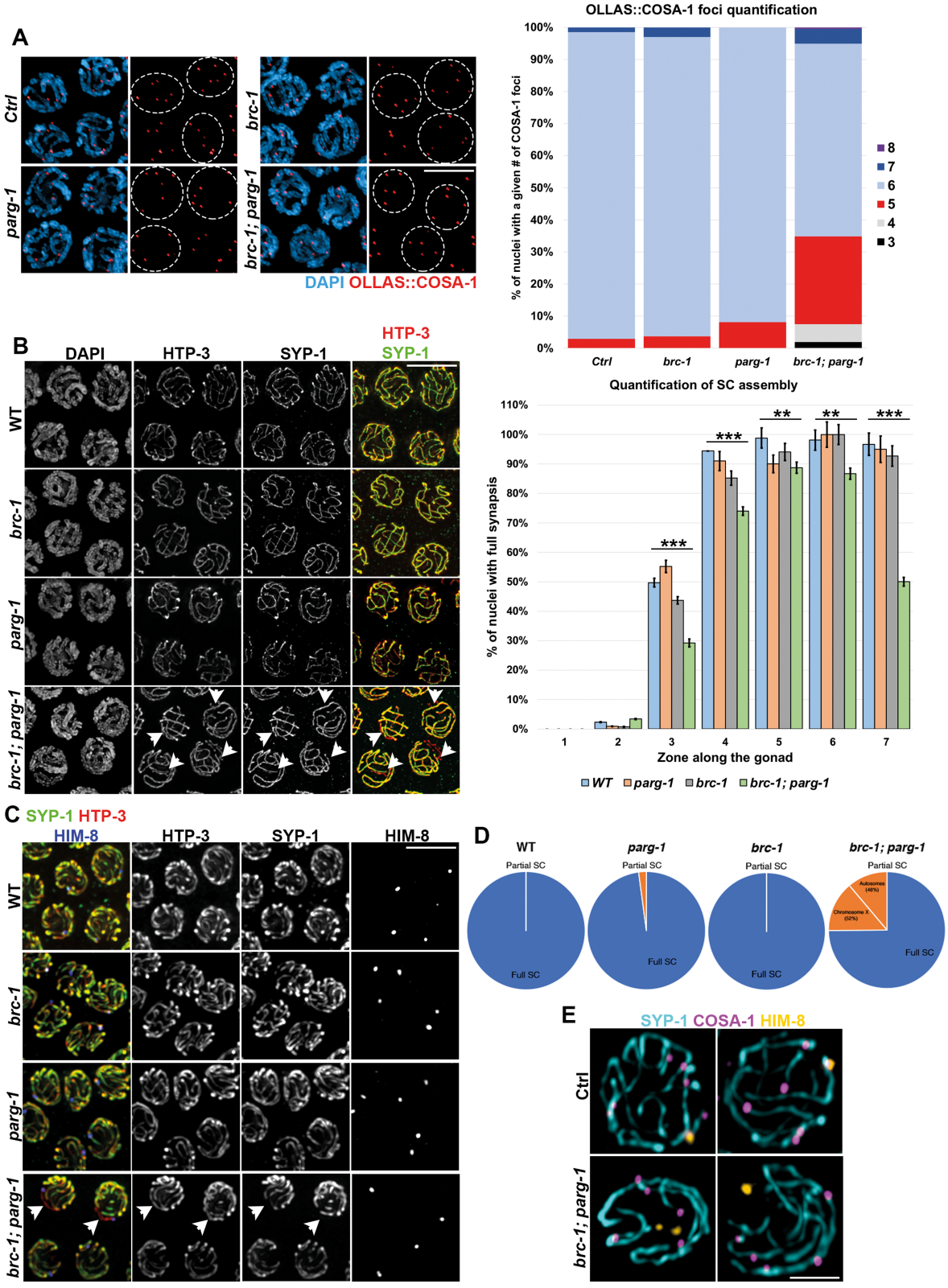

Figure 3. BRC-1-PARG-1 promote robust CO establishment. (**A**) Left: representative images of mid-late pachytene nuclei of the indicated genotypes stained for OLLAS::COSA-1 and DAPI. Dotted circles in the red-channel panels indicate nuclei on the left. Right: quantification of OLLAS::COSA-1 foci number in the last seven rows before diplotene entry. Scale bar 5 μm. (**B**) Left: representative images of mid-late pachytene nuclei stained for HTP-3/SYP-1 in the indicated genotypes. Arrow heads indicate unsynapsed regions. Right: quantification of SC assembly throughout the gonad in the indicated genotypes. Bars show mean ± SEM and asterisks indicate statistically significant differences as calculated by the X^2 test (***$P < 0.0001$, **$P = 0.0036$). Scale bar 5 μm. (**C**) Representative images of mid-late pachytene nuclei stained for HTP-3/SYP-1/HIM-8 in the indicated genotypes. Arrow heads indicate unsynapsed chromosome X. Scale bar 5 μm. (**D**) Pie charts showing fraction of nuclei with full (blue) or partial (orange) SC. (**E**) Representative images of late pachytene nuclei from controls and *brc-1; parg-1* double mutants stained for SYP-1, COSA-1 and HIM-8. Scale bar 5μm.

that peak above wild type levels in early/mid-pachytene but then dissipate by late pachytene stage as in wild type worms (11). Immunostaining of RAD-51 in the *brc-1; parg-1* double mutants mostly recapitulated the expression profile observed in the *brc-1* single mutants (Figure 2E). The notable exception was in the late pachytene stage, where a further increase in the number of RAD-51 foci was observed (Figure 2E, zones 6–7).

To be efficiently loaded in meiotic cells, RAD-51 requires DSB induction (23–26,36,37), presence of single stranded DNA generated upon DSB resection by the MRN/X complex (7,32), and factors that actively promote its loading onto the DNA such as BRCA2/BRC-2 (4,6). To assess whether aberrant RAD-51 loading was caused by perturbations in any of these steps, we analysed localization of i) DSB-1, required for normal DSB induction, ii) MRE-11 and RAD-50, both belonging to the MRN/X complex and iii) BRC-2. We employed available tools for the analysis of MRE-11 (38), while functional RAD-50, DSB-1 and BRC-2 tagged lines (Supplementary Figure S2A-B) were generated by CRISPR/Cas9 for this study.

DSB-1, together with DSB-2/-3, has been shown to be essential for DSB induction presumably by promoting a chromatin environment competent for break formation (23,24,39). Perturbed DSB induction or recombination triggers extended expression of DSB-1 until mid-late pachytene, most likely to prolong the 'window of opportunity' underlying DSB proficiency. Cytological analysis showed that neither *brc-1* nor *parg-1* are required for initial DSB-1 loading. However, DSB-1 localization persisted until the mid-pachytene stage in both the *brc-1* and *parg-1* single mutants, as well as in the *brc-1; parg-1* double mutants (Supplementary Figure S3A), consistent with a defect in DNA repair and suggestive of break formation competence (23,24,39).

Detection of BRC-2 was previously performed with an antibody directed against the endogenous protein, which showed prominent loading of BRC-2 only upon irradiation (4). Our functional *FLAG::brc-2* line however, indicates that BRC-2 is also expressed under physiological conditions of growth at all stages of meiotic prophase I, where it abundantly accumulates in the nucleus (Supplementary Figure S3B). We detected no gross differences in the loading or localization of BRC-2 or MRE-11 and RAD-50 (Supplementary Figure S4A, B), indicating that the defects in the RAD-51 loading observed in the *brc-1; parg-1* double mutants are likely to originate downstream of both DSB induction and resection.

Prior to RAD-51 loading, resected ssDNA is coated with RPA, which binds and stabilizes the DNA filaments before being replaced with RAD-51 (31–33,40–42). Immunostaining analysis revealed that strikingly, while OLLAS::RPA-1 (43) in *brc-1; parg-1* double mutants was loaded until late pachytene stage as in the controls, it did not disengage from DNA at pachytene exit as in WT animals but it rather accumulated in discrete chromatin-associated foci throughout diplotene and diakinesis stages (Figure 2F). These results further corroborate that DSBs are formed and resected in absence of BRC-1 and PARG-1 but their downstream processing is severely impaired, as presence of chromatin-associated RPA-1 foci indicates lingering ssDNA that does not undergo repair.

BRC-1 and PARG-1 cooperate to ensure robust crossover formation

Given the aberrant processing of the recombination intermediates and the increased number of DAPI-bodies in diakinesis nuclei, we next addressed whether establishment of COs was affected in *brc-1; parg-1* double mutants by assessing loading of the pro-CO factor COSA-1, which labels the CO designation sites and is essential for their formation (29). In wild type, COSA- 1 marks six foci in late pachytene nuclei, corresponding to one CO-designation site per chromosome. By contrast, immunofluorescence analysis revealed that only ∼60% of the *brc-1; parg-1* late pachytene nuclei displayed the wild-type complement of six COSA-1 foci. The remainder of the cells had an aberrant number of foci, with the vast majority showing five COSA-1 foci, indicative of the lack of a single CO designation site (Figure 3A).

It has been previously shown that reduced CO numbers trigger the precocious removal of synapsis along the chromosomes that failed to recombine (44,45). Therefore, we sought to investigate whether the defective COSA-1 loading was coupled with the untimely removal of the SC in the *brc-1; parg-1* doubles. To this end, we monitored the pattern of SYP-1 and HTP-3 proteins, which localize to the central elements of the SC and to the chromosome axes, respectively (31,46). As shown in Figure 3B, establishment of the SC was slower in *brc-1; parg-1* doubles compared to wild-type and both single mutants. Upon reaching late pachytene stage (spanning end of zone 6 and overlapping with zone 7), half of the cells displayed chromatin regions stained by HTP-3 but not SYP-1, indicating lack of synapsis. Further, co-staining of the SC and OLLAS::COSA-1 revealed that nuclei displaying de-synapsis carried reduced number of CO designation sites (Supplementary Figure S5), confirming that absence of both BRC-1 and PARG-1 reduces crossover efficiency.

Next, we sought to investigate whether the lack of CO and the consequent untimely removal of the SC were occurring randomly or specifically affecting one chromosome pair. To this end, we monitored the localization of SYP-1, as well as of HIM-8, which binds the sub-telomeric region of the chromosome X (47). If lack of CO was stochastic, we would expect to find desynapsis of the chromosome X in roughly 1/6 of the nuclei, since in *C. elegans* there are six pairs of homologous chromosomes. Interestingly, we found that ∼50% of oocytes that displayed premature loss of SYP-1 were co-labelled with HIM-8 indicating preferential desynapsis along the X chromosome (Figure 3C, D). These chromosomes consistently displayed the expected lack of COSA-1 loading (Figure 3E). This indicates that the pro-HR activity exerted by the combined action of BRC-1 and PARG-1 is particularly important to establish CO designation sites along the sex chromosomes.

Abrogation of cNHEJ triggers accumulation of RAD-51 in *brc-1; parg-1* mutants and mildly reduces embryonic lethality

During gametogenesis, utilization of potential error-prone pathways for DSB repair is normally prevented and a strong homolog-bias ensures faithful chromosome segregation and maintenance of genome integrity through conser-

vative, 'error-free' DNA repair mechanisms such as HR. However, when HR is impaired, cells resort to other DNA repair mechanisms to ensure repair of the damage (4,33,34). Whether this occurs as an active regulatory process or it is instead due to a direct constraint imposed by the presence of factors operating within the HR pathway, is still unclear (33,48). Unlike HR, canonical non-homologous end joining (cNHEJ) relies on break-protection and as such, it does not require end-resection. In worms, it proceeds through DSB stabilization operated by the KU70-KU80 heterodimer (*C. elegans* CKU-70-CKU-80) and Ligase IV-mediated sealing of the breaks (5). Having established that HR is partially compromised in the *brc-1; parg-1* double mutants, we wanted to address whether cNHEJ contributes to genome instability in this background. To this end, we generated the *brc-1 cku-70; parg-1* triple mutants and analysed RAD-51 staining and diakinesis phenotypes. Previous studies have shown that illegitimate activation of KU-dependent end-joining can cause embryonic lethality and hinder the formation of HR-dependent recombination intermediates during meiotic prophase, leading to reduced numbers of RAD-51 foci that can be restored (to different extents) by abrogation of *cku-70/80* function (4,6,33). Assessment of viability levels in the *brc-1 cku-70; parg-1* triple mutants revealed that abrogation of cNHEJ results in a mild, although statistically significant amelioration of embryonic viability (Figure 4A). Interestingly, we found that removal of cNHEJ from both the *brc-1* and *parg-1* single mutants slightly increased embryonic lethality. These results together suggest that while cNHEJ is beneficial and promotes fertility in the *brc-1* and *parg-1* single mutants, it is detrimental when both BRC-1 and PARG-1 are absent (Figure 4A).

Analysis of RAD-51 in the *brc-1 cku-70; parg-1* triple mutants revealed a dramatic increase in the number of foci in late pachytene nuclei (Figure 4B, zone 7), suggesting that removal of cNHEJ redirects a large amount of breaks into a RAD-51-mediated repair pathway. Surprisingly, the increase in RAD-51 loading did not appear to be coupled with a significant improvement of bivalent formation, since analysis of the diakinesis nuclei in the *brc-1 cku-70; parg-1* triple mutants did not reveal obvious differences compared to the *brc-1; parg-1* doubles (Figure 4C). The fact that aberrant DAPI bodies are still formed despite engagement of RAD-51, may suggest the accumulation of intermediates that cannot be fully processed via HR in the *brc-1 cku-70; parg-1* triple mutants or the use of single-strand annealing or break induced replication, which also utilize RAD-51.

POLQ-1 is essential for viability in absence of *brc-1* and *parg-1*

Alternative non-homologous end joining (aNHEJ), also known as TMEJ (Theta-mediated end joining) is independent of the Ku complex and instead requires DNA polymerase Theta/POLQ (*C. elegans* POLQ-1) (49). TMEJ operates in presence of microhomology regions and consequently it carries an intrinsic mutagenic potential.

In order to address whether TMEJ plays a role in the *brc-1; parg-1* double mutant strain, we constructed the *brc-1 polq-1; parg-1* triple mutant strain and performed a similar analysis as for the *brc-1 cku-70; parg-1* mutants. Removal of *polq-1* in *brc-1; parg-1* resulted in near complete embryonic lethality (>90%, compared to ∼60% in *brc-1; parg-1* double mutants) (Figure 5A). Strikingly, abrogation of *polq-1* functions in *brc-1* mutants caused synthetic embryonic lethality with a high variability amongst animals, reaching complete lethality in 15% of the animals screened (6/40) and suggesting that in absence of BRC-1, *polq-1* is important to maintain fertility. Removal of *polq-1* in *parg-1* worms increased embryonic lethality, albeit to a lesser extent than in *brc-1*, indicating that POLQ-1 exerts some roles in a *parg-1*-depleted background.

Analysis of diakinesis nuclei revealed a significant increase in the number of DAPI bodies in the *brc-1 polq-1; parg-1* triple mutants compared to the *brc-1; parg-1* doubles, indicating that loss of POLQ-1 results in increased chromosome fragmentation and/or formation of univalents (Figure 5B). However, chromosome morphology was generally compromised as observed in the *brc-1; parg-1* double mutants, suggesting that formation of these chromatin figures is not dependent on *polq-1* activity.

Surprisingly, we did not find superficial aberrations in chromosome morphology or number in the *brc-1 polq-1* worms despite the high levels of embryonic lethality (Figure 5B), suggesting there may be cytologically undetectable chromosome aberrations or impaired chromosome segregation at later stages.

Loss of POLQ-1 weakens HR-mediated repair in *brc-1; parg-1* double mutants

Given the elevated embryonic lethality and increased number of diakinesis DAPI bodies in *brc-1 polq-1; parg-1* triple mutants, we sought to monitor establishment and resolution of the recombination intermediates by analysing RAD-51 dynamics. This revealed a significant reduction in the mean number of RAD-51 foci compared to *brc-1; parg-1* doubles in early-mid pachytene (zones 4–6), but not in late pachytene (zone 7). Furthermore, we noticed that while not having an effect in the *parg-1* mutants, removal of *polq-1* in the *brc-1* mutants triggered accumulation of high levels of RAD-51 throughout the gonad (Figure 5C) compared to *brc-1* single mutants (Figure 2C).

We then sought to ascertain whether the impact on RAD-51 correlated with a defect in CO-designation as measured by COSA-1 recruitment. Strikingly, the *brc-1 polq-1; parg-1* triple mutants displayed dramatically reduced numbers of COSA-1 foci in comparison to the *brc-1; parg-1* and *brc-1 polq-1* double mutants, indicating that POLQ-1 helps to promote formation of repair intermediates that are proficient in COSA-1 loading when BRC-1 and PARG-1 functions are compromised (Figure 5D). Consistent with the reduced CO competence, we found that significant levels of desynapsis were found in late pachytene (Supplementary Figure S6). We note that SC assembly in the *brc-1 polq-1; parg-1* mutants occurred much more slowly than in the *brc-1; parg-1* doubles at earlier stages, however it reached comparable levels in late pachytene (Supplementary Figure S6).

Given the reduced levels of HR-mediated repair, we wondered whether aberrant chromosome figures in the diakinesis nuclei resulted from non-homologous chromosome fusions. To address this possibility, we performed FISH anal-

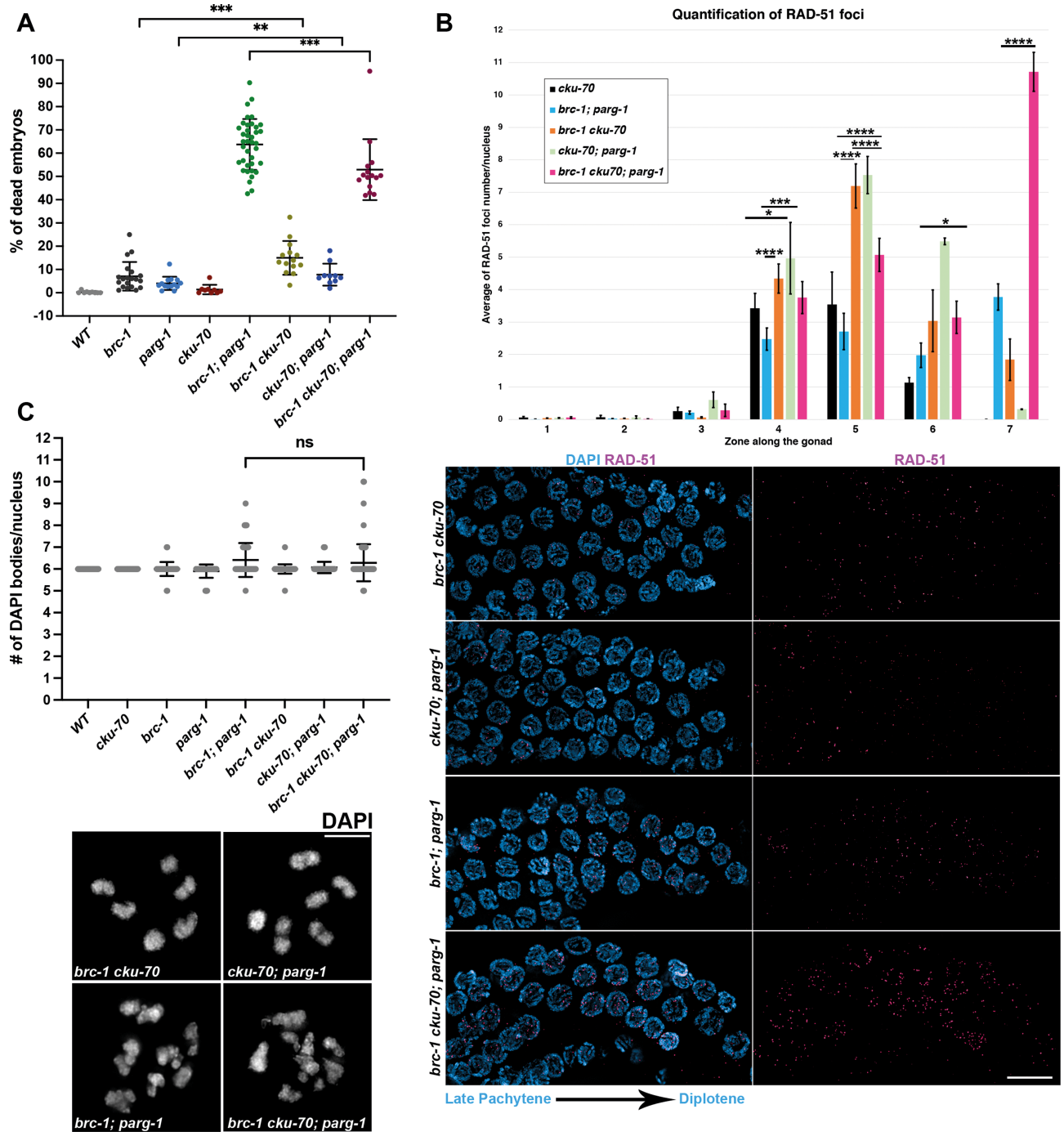

Figure 4. Abrogation of cNHEJ mildly improves viability in *brc-1; parg-1* doubles. (**A**) Quantification of embryonic lethality in the indicated genotypes. Bars indicate mean ± SD and asterisks denote statistical significance as calculated by the *t* test (***$P < 0.0001$, **$P = 0.0068$). (**B**) Top: quantification of RAD-51 foci number in the indicated genotypes across the gonad. Bars show mean ± SEM and asterisks denote statistical significance as calculated by the *t* test (Zone 4: ****$P < 0.0001$, ***$P = 0.0002$, *$P = 0.03$; Zone 5: ****$P < 0.0001$; Zone 6: *$P = 0.02$; Zone 7: ****$P < 0.0001$). Bottom: representative images of late pachytene regions from gonads of the indicated genotypes, stained for RAD-51 and DAPI. Scale bar 10 μm. (**C**) Top: quantification of DAPI bodies in the indicated genotypes. Bars indicate mean ± SD. Bottom: representative images of diakinesis nuclei of the indicated genotypes (^{ns}*non-significant* as calculated by *t* test). Scale bar 5μm.

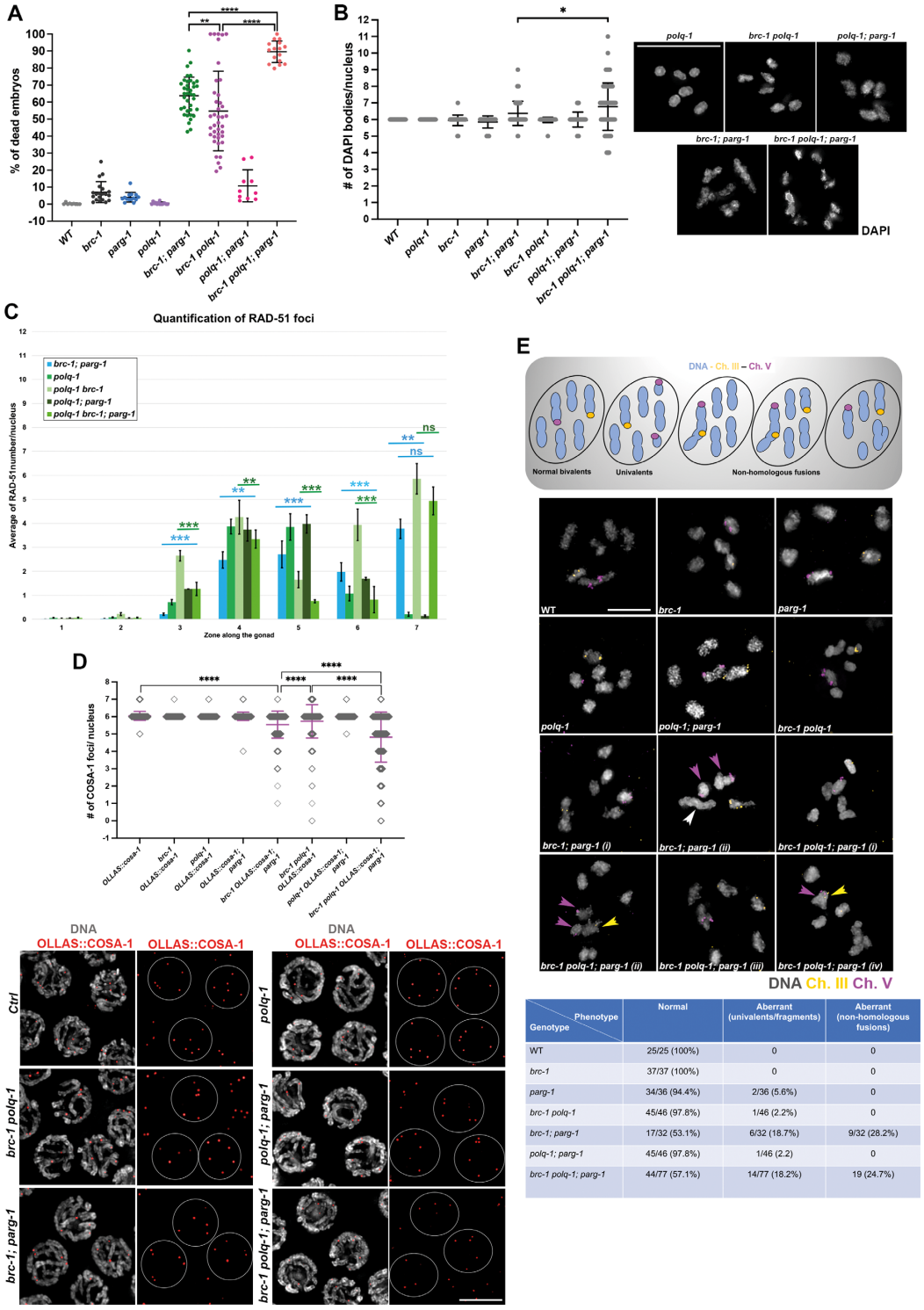

Genotype \ Phenotype	Normal	Aberrant (univalents/fragments)	Aberrant (non-homologous fusions)
WT	25/25 (100%)	0	0
brc-1	37/37 (100%)	0	0
parg-1	34/36 (94.4%)	2/36 (5.6%)	0
brc-1 polq-1	45/46 (97.8%)	1/46 (2.2%)	0
brc-1; parg-1	17/32 (53.1%)	6/32 (18.7%)	9/32 (28.2%)
polq-1; parg-1	45/46 (97.8%)	1/46 (2.2)	0
brc-1 polq-1; parg-1	44/77 (57.1%)	14/77 (18.2%)	19 (24.7%)

Figure 5. Preventing Theta-mediated function results in synthetic lethality in *brc-1* and *brc-1; parg-1* mutants. (**A**) Quantification of embryonic lethality in the indicated genotypes. Bars indicate mean ± SD and asterisks denote statistical significance as calculated by *t* test (****$P < 0.0001$, **$P = 0.002$). (**B**) Quantification of DAPI bodies in the indicated genotypes and representative images on the right. Bars show mean ± SD and *$P = 0.03$ as calculate by *t* test. (**C**) Quantification of RAD-51 foci number in the indicated genotypes. Bars show mean ± SEM and asterisks indicate statistical significance (Zone 3: ***$P < 0.0001$; Zone 4: **$P = 0.003$; Zone 5: ***$P < 0.0001$; Zone 6: ***$P < 0.0001$, Zone 7: **$P = 0.0032$, ^{ns}*non-significant*) as calculated by *t* test. (**D**) Quantification (top) and representative images of late-pachytene nuclei stained for OLLAS::COSA-1 and DAPI (bottom) in the indicated genotypes. Scale bar 5μm. Bars show mean ± SD and asterisks denote statistical significance as calculated by the *t* test (****$P < 0.0001$). (**E**) Top: schematic representation of possible outcomes obtained by FISH analysis. Middle: representative images of FISH analyses on diakinesis nuclei in the indicated genotypes. Arrowheads are color-coded according to the probe that they are indicating. White arrowhead points at non-homologous fusion that does not involve chromosomes III and V. Two examples are provided for *brc-1; parg-1* double mutants and four for the *brc-1 polq-1; parg-1* triple mutants. Scale bar 5μm. Bottom: table reporting frequency of chromosomal aberrancies in the indicated genotypes.

ysis with specific probes recognizing autosomes III and V and determined DAPI-body identities in the *brc-1; parg-1* double and *brc-1 polq-1; parg-1* triple mutants and relevant controls (Figure 5E). In wild-type, each bivalent is marked by a single focus (or a very tight doublet) corresponding to the sequence recognized by the probe. In case univalents or fragments are present, two or more DAPI bodies will be labelled by each probe, respectively. This technique will underestimate the rates of chromosome fragmentation events since one can only interrogate the chromosomal regions from the probe site to the end of the chromosome. If non-homologous fusions have arisen between the chromosomes recognized by the probes, both signals will be detected within the same chromatin mass. We found that in *brc-1; parg-1* and *brc-1 polq1; parg-1*, 46.8% and 42.8% of the diakinesis nuclei contained non-homologous fusions, respectively (Figure 5E). These results further corroborate that DSB repair is severely deregulated in absence of these factors.

Consistent with major defects present in diakinesis oocytes of *brc-1 polq-1; parg-1*, we also observed higher numbers of RPA-1 foci in diplotene and diakinesis nuclei compared to the *brc-1; parg-1* doubles (Figure 6). Importantly, analysis of *brc-1 polq-1* double mutants also revealed substantial accumulation of RPA-1 foci in diplotene and diakinesis nuclei. This supports our genetic data that shows essential requirements imposed by *polq-1* function in safeguarding genome stability in a *brc-1*-compromised background.

PARG-1 catalytic activity partially safeguards genome integrity in absence of *brc-1* but is not essential for establishment of COs

We have previously shown that PARG-1 loading along the chromosomes and its catalytic activity in removing poly(ADP) ribose (PAR) moieties play differential roles during gametogenesis in worms. Loading of PARG-1 is essential to promote DSB induction and HR-mediated repair, whereas PARG-1 catalytic activity has an effect in regulating the protein turn over and is not required for recombination (11).

Given the synthetic effects found in the *brc-1; parg-1* double mutants, we sought to investigate whether the lack of PARG-1 catalytic activity or defects in its loading were the underlying cause of the observed defects. To this end, we combined the *parg-1* catalytic-dead mutant allele that we previously generated (11) (called *parg-1(CD)* hereafter to distinguish it from the *parg-1(gk120)* null allele) with *brc-1* null mutants and reassessed embryonic viability. We found that abrogation of PARG-1 catalytic activity in *brc-1* mutants caused a 3-fold increase in the embryonic lethality. However, the percentage of dead embryos was roughly half compared to *brc-1; parg-1(gk120)* null worms (Figure 7A), suggesting that loss of the catalytic activity alone cannot explain the embryonic lethality.

Given the defects in the establishment of CO-designation sites and the precocious desynapsis observed in the *brc-1; parg-1(gk120)* double mutants (Figure 3), we wanted to assess whether the embryonic lethality in *brc-1; parg-1(CD)* could also result from incomplete synapsis and/or reduced recombination. To this end, we monitored SC dynamics and crossover designation events in the *brc-1; parg-1(CD)* double mutants. Unlike the *brc-1; parg-1(gk120)* (Figure 3), we did not observe desynapsis (Supplementary Figure S7A) or defects in COSA-1 foci number (Supplementary Figure S7B, C), indicating that the PARG-1 catalytic activity is dispensable for normal levels of synapsis and recombination upon lack of BRC-1.

Abrogation of *parp-1/2* function triggers dichotomous effects in *brc-1; parg-1(gk120)* and *brc-1; parg-1(CD)* mutant backgrounds

Given that PARG-1 catalytic activity contributes to embryonic lethality, we hypothesized that loss of the poly(ADP)ribose polymerases PARP-1 and PARP-2 (11,50) would suppress the lethality defects. Therefore, we generated the *parp-1; parp-2; brc-1; parg-1(CD)* quadruple mutants. Contrary to our expectation, loss of PARP activities failed to rescue or attenuate the embryonic lethality seen in *brc-1; parg-1(CD)*, but strikingly, further reduced viability (Figure 7A). Removal of *parp-1/-2* elicited a similar synthetic effect in the *brc-1; parg-1(gk120)*. These results indicate that while accumulation of PAR due to impaired catalytic activity or *parg-1* knockout exerts toxic effects in *brc-1* mutants, its absence confers even more severe consequences. Interestingly, we observed a dramatic reduction in the brood-size of *brc-1; parg-1(CD)* double mutants, which was not present in the *brc-1; parg-1(gk120)* and that was suppressed by contemporaneous removal of *parp-1* and *parp-2* (Figure 7B). Moreover, we noticed that both quadruple mutants displayed a stark growth delay compared to the other strains (Supplementary Figure S8), pointing at possible repair defects in the somatic cells as well (5).

We proceeded to analyse DAPI bodies in diakinesis nuclei, as well as RAD-51 loading dynamics in the two quadruple mutants. While embryonic lethality was proportionally enhanced in both *parp-1; parp-2; brc-1; parg-1(CD)* and *parp-1; parp-2; brc-1; parg-1(gk120)* quadruple mutants (Figure 7A), we found a phenotypic dichotomy when we monitored RAD-51 loading and chromosome morphology/number. In fact, the *parp-1; parp-2; brc-1; parg-1(CD)* worms exhibited increased RAD-51 foci throughout the gonad compared to the *brc-1; parg-1(CD)*, suggesting a PAR-dependent effect in reducing RAD-51 loading, and we did not find alterations in the number and the morphology of the DAPI bodies (Figure 7D–G). On the other hand, removal of the PARPs from the *brc-1; parg-1(gk120)* double mutants reduced and flattened RAD-51 foci number at all stages in comparison to the *brc-1; parg-1(gk120)* doubles (Figure 7E–G). This was also coupled with enhanced frequency of chromosomal aberrations in the diakinesis nuclei (Figure 7D versus Figure 2C).

Altogether, these results clearly demonstrate that both PARG-1 catalytic activity and its 'structural' roles along the chromosomes are required at different steps during gametogenesis and their impairment elicits different outcomes in combination with other defective branches of meiotic DSB

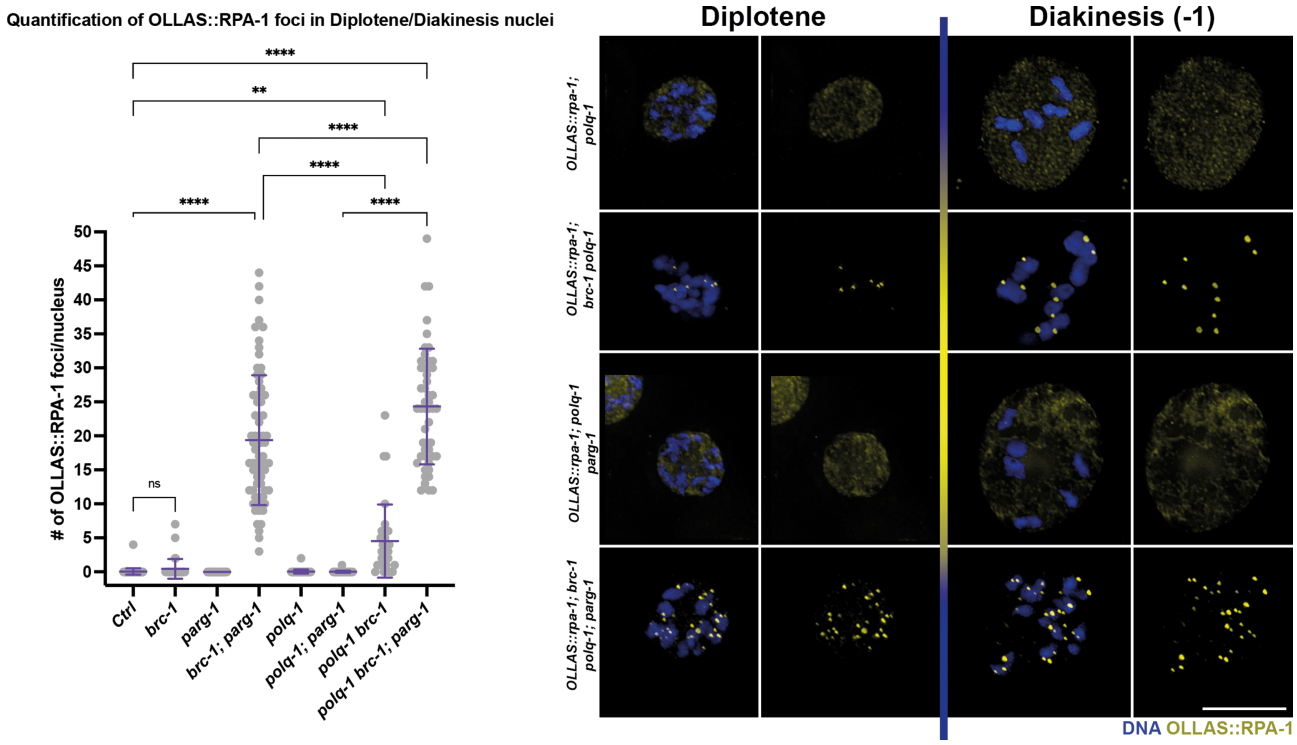

Figure 6. Lack of POLQ-1 enhances RPA-1 foci formation in Diplotene and Diakinesis nuclei. Left: quantification of OLLAS::RPA-1 foci in the indicated genotypes. Each circle represents one nucleus. Bars indicate Mean ± SD. Asterisks denote statistical significance as calculated by one-way ANOVA (****$P < 0.0001$; **$P = 0.0017$). Right: representative images of nuclei stained for OLLAS::RPA-1 and counterstained by DAPI in the indicated stages and genotypes. Scale bar 2 μm.

repair as evidenced by coincident lack of BRC-1. Further studies will be necessary to clarify how the ambivalent functions of PARG-1 differentially operate in developing gametes and how these intersect BRCAs′ in acting as safekeepers of genome integrity in the germ line.

DISCUSSION

ADP-ribosylation is a crucial post-translational modification that plays pivotal roles during DNA repair. The founder 'writers' and 'erasers', PARP1/2 and PARG respectively, have been extensively studied in mitotic cell culture models, however their characterization during gametogenesis has received significantly less attention, since mice mutants of PARG and double knockouts of PARP1/2 are embryonic lethal (51–55), hindering their study in the germ line.

Inhibition of poly(ADP)-ribosylation (PARylation) in cancer cells harbouring mutations in the BRCA1/2 genes elicits synthetic lethality due to impaired repair of DSBs arising from the collision of the replication forks with trapped PARP1-DNA adducts. This synthetic lethality is currently exploited in cancer therapy (56–59). A similar approach aimed at targeting PARG has proved to be more problematic, due to lower specificity and high toxicity of available chemical inhibitors (59). Therefore, whether impairment of PARG function in BRCAs-mutated cells elicits the same phenotypes observed for PARPs inhibition, is still under debate.

PARG holds crucial functions for repair and recombination in BRCA1/BARD1-mutated backgrounds

We show that abrogating PARG function in null *brc-1* mutant worms causes high embryonic lethality due to aberrant DNA repair and weakened CO establishment in developing oocytes. Contemporaneous loss of *brc-1* and *parg-1* results in the formation of aberrant chromosome structures in the diakinesis nuclei, indicating that BRC-1 and PARG-1 are likely to act in distinct pathways during meiotic progression.

Interestingly, we found that fertility is progressively compromised with aging in *brc-1; parg-1* double mutants, further corroborating previous evidence showing a stark decline of gametes quality in mutants with defective meiotic recombination and dysfunctional DNA repair, which consequently become hypersensitive to the detrimental effects of aging on genome stability (60–62).

Abrogation of *brc-1* function perturbs RAD-51 loading in the *C. elegans* gonad, where it accumulates in chromatin-associated foci at late pachytene stage (10). In contrast, in *parg-1* mutants the number of RAD-51-labeled recombination intermediates rises above WT levels at early-mid pachytene stages (11). In early pachytene, *brc-1* is epistatic to *parg-1* intimating that BRC-1 acts upstream of PARG-1 in formation/processing of recombination intermediates. By contrast *brc-1* and *parg-1* show a synthetic effect - increased RAD-51 accumulation - in late pachytene. The early, reduced numbers of RAD-51 foci number in *brc-1; parg-1* versus *parg-1* mutants is unlikely to originate from impaired DSB formation or reduced end-resection,

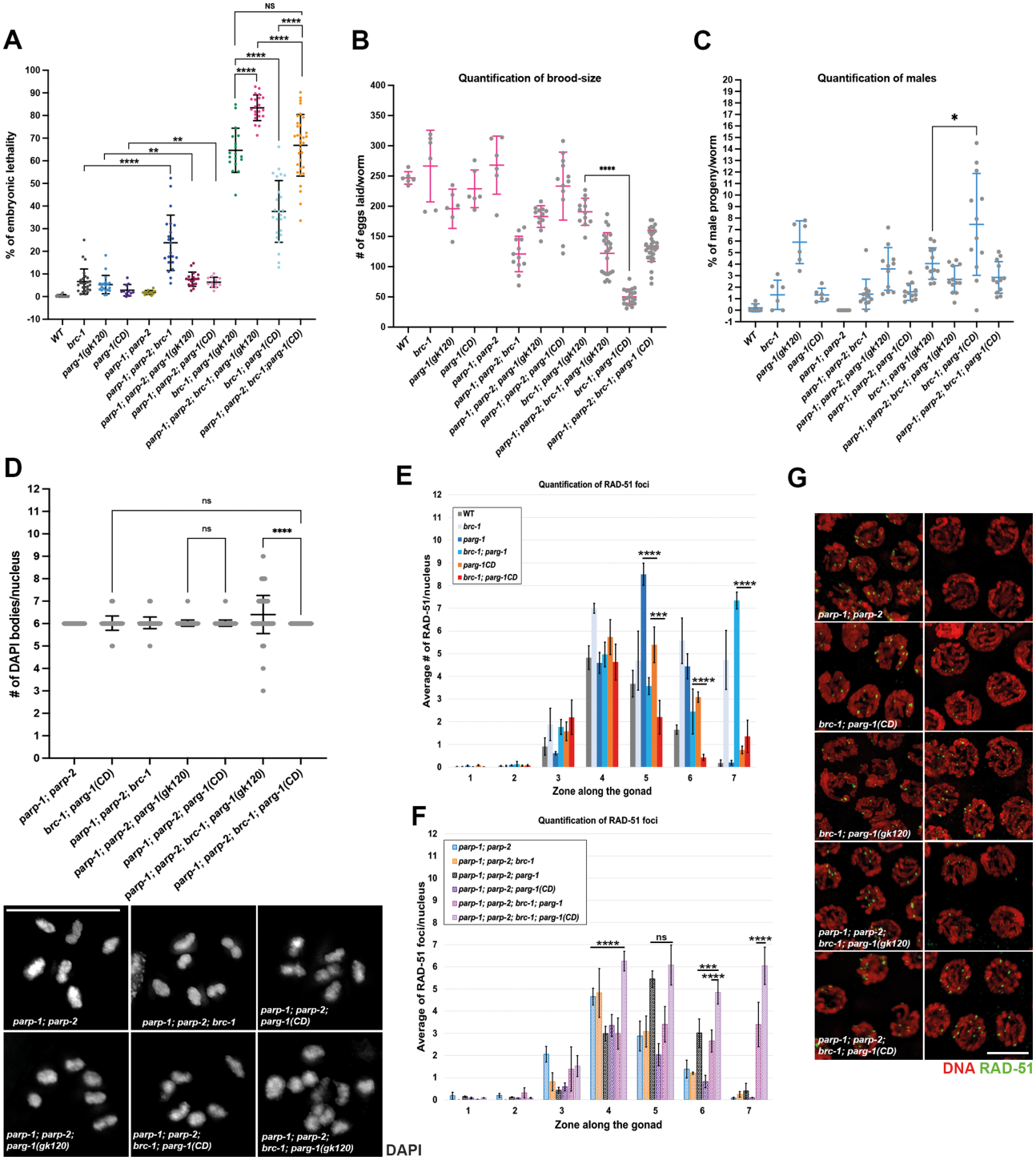

Figure 7. PARG-1 catalytic activity is partially required to avert genome instability in absence of *brc-1*. (**A**) Quantification of embryonic lethality in the indicated genotypes. Bars show mean ± SD and asterisks indicate statistical significance as calculated by Mann–Whitney test (***$P < 0.0001$, **$P = 0.0002$, ^{ns}*non-significant*). (**B**) Quantification of brood-size in the indicated genotypes. Bars report mean ± SD. ****$P < 0.0001$ as calculated by Mann–Whitney test. (**C**) Quantification of male progeny in the indicated genotypes. Bars report mean ± SD. *$P = 0.028$ as calculated by Mann–Whitney test. (**D**) Top: quantification of DAPI-stained bodies in the indicated genotypes. Bars show mean ± SD and asterisks indicate statistical significance as calculated by *t* test (****$P < 0.0001$; ^{ns}*non-significant*). Bottom: representative images of diakinesis nuclei from the indicated genotypes. Scale bar 3 μm. (**E**, **F**) Quantification of RAD-51 foci number and (**G**) representative images of late pachytene nuclei in the indicated genotypes. Bars show mean ± SEM and asterisks denote statistical significance as assessed by the *t* test (****$P < 0.0001$, ***$P = 0.00033$, ^{ns}*non-significant*). Scale bar 5 μm.

since we found that loading of the pro-DSB factor DSB-1 and the MRN complex components MRE-11 and RAD-50 are comparable to wild-type controls. Our data indicate that meiotic DSBs are formed in absence of *brc-1* and *parg-1* but are not efficiently repaired, as further corroborated by a) normal RPA-1 loading, but impaired removal, and b) the appearance of nonhomologous chromosome fusions in diakinesis nuclei which require *spo-11* activity. While we cannot rule out that impaired RPA-1 removal is caused by hindered exchange with RAD-51 *per se*, we think this data rather points to a scenario whereby some SPO-11-dependent DNA lesions formed in absence of BRC-1/PARG-1 cannot be processed by HR and consequently are hijacked by multiple illegitimate error-prone pathways.

It has been postulated that BRC-1 activity promotes non-crossover-mediated repair and that in its absence, delayed recombination intermediates may be channelled into alternative forms of repair (10). PARG-1 could be involved in promoting such alternative repair pathway(s), although it is worth mentioning that a large proportion of nuclei in the *brc-1; parg-1* double mutants display a normal complement of bivalents in the diakinesis nuclei, as well as proper number of CO-designation sites, indicating that PARG-1 could act on a subset of recombination intermediates. Intriguingly, we find that lack of COs is particularly prominent on the chromosome X, suggesting that PARG-1 functions in promoting recombination might be required to different extents between autosomes and sex chromosomes. This is consistent with our previous finding that in *him-5* mutants, which are defective in forming COs on the chromosome X but not on the autosomes, lack of *parg-1* weakens IR-dependent rescue of chiasmata (11).

The X chromosome has unique histone modifications (63), recombination rates (25,37,64) and DSB proficiency (65,66) compared to autosomes. Therefore, it may be more prone to CO defects caused by perturbed DNA repair directly or perhaps reduced DSB formation.

POLQ as a crucial resource for survival upon BRCA1- and BRCA1-PARG-deficiencies

Our data unveil a complex, multi-layered control exerted by BRC-1 and PARG-1 on DNA repair pathway choice that intersects both cNHEJ and TMEJ pathways and whose functional ramifications differently impact HR-mediated repair. Preventing Ku-mediated cNHEJ induces a dramatic accumulation of RAD-51 foci in late pachytene cells, yet mildly alleviates embryonic lethality in the *brc-1; parg-1* double mutants. This does not improve chromosome morphology in the diakinesis nuclei. On the other hand, removal of *polq-1* causes high embryonic lethality in *brc-1* mutants and complete embryonic lethality in the *brc-1; parg-1*, indicating that in absence of BRC-1, TMEJ is essential to maintain fecundity. Surprisingly, we did not find obvious alterations in the morphology or number of DAPI bodies in *brc-1 polq-1* double mutants despite the high level of embryonic lethality. This could indicate that the outcome of the aberrant repair taking place in these double mutants may not be detectable at the level of chromosome morphology in the diakinesis nuclei, that such defects might be revealed at later stages of meiotic progression such as in Metaphase I-Anaphase I (e.g. lagging chromosomes, chromatin bridges), preventing proper chromosome segregation, or that these genes have additional and essential roles in embryogenesis. Interestingly, the number of RAD-51 foci was increased across the germ lines of the *brc-1 polq-1* double mutants, suggesting that removal of POLQ-1 triggers accumulation of recombination intermediates at all stages of Prophase I.

Previous work has shown that lack of *brc-1* triggers transgenerational accumulation of mutations in a *polq-1*-dependent fashion (67), thus the worsening in the viability levels that we observe when *polq-1* is removed from *brc-1* mutants seems rather counterintuitive. However, it is possible that while abrogating *polq-1* function in a *brc-1*-deficient background suppresses its mutagenic potential, at the same time it may also affect genome stability by other means. In fact, the *polq-1*-dependent impact on genomic fidelity could arise by other (*polq-1*-independent) sources, that result in the activation of TMEJ as an emergency resource mechanism. Hence, removing POLQ-1 would avert formation of mutations, but at the same time could also suppress an instrumental tool for repairing DNA damage, ultimately resulting in reduced viability. This is further corroborated by formation of RPA-1 foci in diplotene and diakinesis nuclei in the *brc-1 polq-1* double mutants, and even a more dramatic increase was observed in the *brc-1 polq-1; parg-1* triple mutants, suggesting formation of ssDNA that could not undergo proper DNA repair before approaching Metaphase I. In addition, a significant reduction in COSA-1 foci number and precocious desynapsis was also found in *brc-1 polq-1* doubles, indicating reduced HR competence. This phenotype was further exacerbated in the *brc-1 polq-1; parg-1* triple mutants, suggesting that POLQ-1 is responsible for maintaining residual levels of viability in absence of *brc-1* and *parg-1* and to promote establishment of CO-designation sites. The presence of chromosome aberrations upon removal of *cku-70* or *polq-1*, irrespective of the effects on RAD-51 loading, indicates that multiple, mutagenic repair pathways can be engaged in the *brc-1; parg-1* double mutants, resulting in chromosome abnormalities. This further corroborates previous work showing that a plethora of repair mechanisms can act on meiotic breaks within the *C. elegans* germ line with high redundancy (48).

There is more to PARPs-PARG than just synthetizing/degrading PAR

Interestingly, we found that contrary to what we previously observed in *him-5* mutants (11), PARG-1 catalytic activity plays pivotal roles in promoting RAD-51-labeled recombination intermediates in late pachytene cells in absence of *brc-1* and this is correlated with increased embryonic lethality. However, the embryonic lethality in *brc-1; parg-1* null worms is much higher than in *brc-1; parg-1(CD)*. Thus, we can conclude that while PARG-1 catalytic activity plays important roles in promoting repair of late recombination intermediates generated in *brc-1* mutant animals, the protein has additional - likely structural roles - that contribute to its ability to safeguard genome stability in this background. This was further emphasized by unperturbed SC

assembly/disassembly kinetics and normal numbers of CO-designation sites in the *brc-1; parg-1(CD)*.

Nevertheless, absence of rescue or amelioration of viability levels observed upon removal of PAR polymerases PARP-1/2 in the *brc-1; parg-1(CD)* unveiled an unforeseen and much more complex functional crosstalk between the PAR-synthesis and PAR-catabolism pathways than anticipated. Loss of *parp-1* and *parp-2* in both *brc-1; parg-1(CD)* and *brc-1; parg-1* nulls proportionally enhanced embryonic lethality suggesting crucial, PAR-independent but PARPs-dependent roles, for maintaining residual fertility levels. However, in the two quadruple mutants, the establishment and resolution of RAD-51-labelled recombination intermediates displayed inverse dynamics and aberrant diakinesis figures were only observed in the *parp-1; parp-2; brc-1; parg-1* nulls. These results may suggest that the presence of catalytically inactive PARG-1 along the chromosomes (11) limits or prevents RAD-51 loading in a *brc-1*-compromised background due to either accumulation of PAR or *via* PAR-independent functions of PARP-1 and PARP-2. The fact that removal of PARPs from the *brc-1; parg-1(CD)* also significantly improves brood-size may originate from a possible modulation of germ line apoptosis, which has been shown to affect fertility by culling defective oocytes (68), or perhaps may arise from functional defects during spermatogenesis, since the number of fertilized eggs laid by hermaphrodite animals relies on the number of the sperm produced (69).

The extensive presence of diakinesis nuclei displaying chromosome abnormalities in the *parp-1; parp-2; brc-1; parg-1(gk120)* but not in the *parp-1; parp-2; brc-1; parg-1(CD)* could indicate that although not being able to degrade PAR chains, PARG-1^{CD} loading along the chromosomes may still be able to sustain the signalling necessary to complete repair in *brc-1* mutants, highlighting the PAR-independent roles that PARG plays during gametogenesis. It has been previously shown in mammalian cell cultures models that targeting of PARG^{WT} to damage sites generated by laser microirradiation can be independent of PARP1 or PARP2, and is only partially affected by PARP inhibition (70). Further, catalytically inactive PARG was shown to undergo faster recruitment kinetics than wild-type PARG, but its localization was severely affected by PARP inhibitors and to a lesser extent by PARP1 knock-out (70). These data from *ex vivo* models, combined with our analyses *in vivo*, clearly indicate that the functional links between PARPs and PARG are wider and more complex than anticipated and cannot be framed by just antagonistic roles established through PAR-synthesis and PAR-removal. The functions exerted by PARG *in vivo* during gametogenesis have not been investigated and therefore our work has only started to unveil the multifaceted aspects of PARG during meiosis.

In conclusion, our data demonstrate that as observed upon PARPs inhibition in mitotic cells, blocking PARG-1 functions in *brc-1* mutated animals confers synthetic effects. Our work shows that abrogation of PARP-1 and PARP-2 function however, has less dramatic repercussions on *brc-1* mutants than lack of PARG-1, since the *parp-1; parp-2; brc-1* triple mutants are more fertile than the *brc-1; parg-1* doubles. This could be due to the fact that PARPs inhibition and PARPs knockout are likely to elicit very different responses, since in the former instance the proteins remain trapped on the chromatin, whereas in the latter case they are not present in the cells. In fact, this aligns with the findings in human mitotic cells whereby knock down of *PARP1/2* in *BRCA*$^{-/-}$ cells does not elicit the same extent of lethality as upon PARP1 inhibition, indicating that the mechanisms underlying these responses are very likely to be different. We have uncovered an intricate and complex activity mediated by BRC-1 and PARG-1 in regulating DNA repair pathway choice during gametogenesis, with functional ramifications to both HR, as well as NCO-dependent repair, placing these two important factors at a crossroad between multiple routes.

DATA AVAILABILITY

All the relevant data underlying the experiments shown in this study are included in the manuscript. Requests for strains and/or reagents should be addressed to the corresponding author (silva@med.muni.cz).

SUPPLEMENTARY DATA

Supplementary Data are available at NAR Online.

ACKNOWLEDGEMENTS

We are grateful to S. Boulton for the anti-BRD-1 antibody, E. Martinez-Perez for the chicken anti-SYP-1, A. Villeneuve for the *rad-50(ok197)* mutant and S. Smolikove for the *mre-11::GFP* and *OLLAS::rpa-1* strains. We are grateful to Angela Graf and Verena Jantsch for the unvaluable help in generating the *3xHA::dsb-1*, *3xFLAG::brc-2* and *rad-50::3xFLAG* tagged lines, and to Marilina Raices and Judith Yanowitz for their help with editing the manuscript. We acknowledge the core facility CELLIM supported by the Czech- BioImaging large RI project (LM2018129 funded by MEYS CR) for their support with obtaining scientific data presented in this paper. Some of the strains employed in this study were provided by the C.G.C., which is funded by NIH Office of Research Infrastructure Programs (P40 OD010440).

Author contributions: N.S. designed the research; S.T. and N.S. performed the experiments with the technical support of J.B.; N.S. supervised the project and wrote the manuscript.

FUNDING

Research in N.S. lab is funded by the Czech Science Foundation [GAČR, GA20-08819S]; Start-up grant from the Department of Biology of Masaryk University, Faculty of Medicine. Funding for open access charge: Czech Science Foundation.

Conflict of interest statement. None declared.

REFERENCES

1. Zickler,D. and Kleckner,N. (1999) Meiotic chromosomes: integrating structure and function. *Annu. Rev. Genet.*, **33**, 603–754.

2. Zickler,D. and Kleckner,N. (2015) Recombination, pairing, and synapsis of homologs during meiosis. *Cold Spring Harb. Perspect. Biol.*, **7**, a016626.
3. Keeney,S., Giroux,C.N. and Kleckner,N. (1997) Meiosis-specific DNA double-strand breaks are catalyzed by spo11, a member of a widely conserved protein family. *Cell*, **88**, 375–384.
4. Martin,J.S., Winkelmann,N., Petalcorin,M.I.R., McIlwraith,M.J. and Boulton,S.J. (2005) RAD-51-Dependent and -Independent roles of a *Caenorhabditis elegans* BRCA2-Related protein during DNA double-strand break repair. *Mol. Cell. Biol.*, **25**, 3127–3139.
5. Clejan,I., Boerckel,J. and Ahmed,S. (2006) Developmental modulation of nonhomologous end joining in *Caenorhabditis elegans*. *Genetics*, **173**, 1301–1317.
6. Petalcorin,M.I.R., Sandall,J., Wigley,D.B. and Boulton,S.J. (2006) CeBRC-2 stimulates D-loop formation by RAD-51 and promotes DNA Single-strand annealing. *J. Mol. Biol.*, **361**, 231–242.
7. Yin,Y. and Smolikove,S. (2013) Impaired resection of meiotic double-strand breaks channels repair to nonhomologous end joining in *Caenorhabditis elegans*. *Mol. Cell. Biol.*, **33**, 2732–2747.
8. Li,Q. and Engebrecht,J. (2021) BRCA1 and BRCA2 tumor suppressor function in meiosis. *Front. Cell Dev. Biol.*, **9**, 668309.
9. Janisiw,E., Dello Stritto,M.R., Jantsch,V. and Silva,N. (2018) BRCA1–BARD1 associate with the synaptonemal complex and pro-crossover factors and influence RAD-51 dynamics during *Caenorhabditis elegans* meiosis. *PLoS Genet.*, **14**, e1007653.
10. Adamo,A., Montemauri,P., Silva,N., Ward,J.D., Boulton,S.J. and La Volpe,A. (2008) BRC-1 acts in the inter-sister pathway of meiotic double-strand break repair. *EMBO Rep.*, **9**, 287–292.
11. Janisiw,E., Raices,M., Balmir,F., Paulin,L.F., Baudrimont,A., von Haeseler,A., Yanowitz,J.L., Jantsch,V. and Silva,N. (2020) Poly(ADP-ribose) glycohydrolase coordinates meiotic DNA double-strand break induction and repair independent of its catalytic activity. *Nat. Commun.*, **11**, 4869.
12. Brenner,S. (1974) The genetics of *Caenorhabditis elegans*. *Genetics*, **77**, 71–94.
13. Polanowska,J., Martin,J.S., Garcia-Muse,T., Petalcorin,M.I.R. and Boulton,S.J. (2006) A conserved pathway to activate BRCA1-dependent ubiquitylation at DNA damage sites. *EMBO J.*, **25**, 2178–2188.
14. Das,D., Trivedi,S., Blazícková,J., Arur,S. and Silva,N. (2022) Phosphorylation of HORMA-domain protein HTP-3 at serine 285 is dispensable for crossover formation. *G3 Genes|Genomes|Genetics*, **12**, jkac079.
15. Kurhanewicz,N.A., Dinwiddie,D., Bush,Z.D. and Libuda,D.E. (2020) Elevated temperatures cause transposon-associated DNA damage in *C. elegans* spermatocytes. *Curr. Biol.*, **30**, 5007–5017.
16. Silva,N., Ferrandiz,N., Barroso,C., Tognetti,S., Lightfoot,J., Telecan,O., Encheva,V., Faull,P., Hanni,S., Furger,A. *et al.* (2014) The fidelity of synaptonemal complex assembly is regulated by a signaling mechanism that controls early meiotic progression. *Dev. Cell*, **31**, 503–511.
17. Woglar,A., Daryabeigi,A., Adamo,A., Habacher,C., Machacek,T., La Volpe,A. and Jantsch,V. (2013) Matefin/SUN-1 phosphorylation is part of a surveillance mechanism to coordinate chromosome synapsis and recombination with meiotic progression and chromosome movement. *PLoS Genet.*, **9**, e1003335.
18. Paix,A., Schmidt,H. and Seydoux,G. (2016) Cas9-assisted recombineering in *C. elegans*: genome editing using *in vivo* assembly of linear DNAs. *Nucleic Acids Res.*, **44**, e128.
19. Wu,L.C., Wang,Z.W., Tsan,J.T., Spillman,M.A., Phung,A., Xu,X.L., Yang,M.-C.W., Hwang,L.-Y., Bowcock,A.M. and Baer,R. (1996) Identification of a RING protein that can interact in vivo with the BRCA1 gene product. *Nat. Genet.*, **14**, 430–440.
20. Li,Q., Saito,T.T., Martinez-Garcia,M., Deshong,A.J., Nadarajan,S., Lawrence,K.S., Checchi,P.M., Colaiacovo,M.P. and Engebrecht,J. (2018) The tumor suppressor BRCA1–BARD1 complex localizes to the synaptonemal complex and regulates recombination under meiotic dysfunction in *Caenorhabditis elegans*. *PLos Genet.*, **14**, e1007701.
21. Hodgkin,J., Horvitz,H.R. and Brenner,S. (1979) nondisjunction mutants of the nematode *Caenorhabditis elegans*. *Genetics*, **91**, 67–94.
22. Hillers,K.J. (2017) Meiosis. *WormBook*, https://doi.org/10.1895/wormbook.1.178.1.
23. Rosu,S., Zawadzki,K.A., Stamper,E.L., Libuda,D.E., Reese,A.L., Dernburg,A.F. and Villeneuve,A.M. (2013) The *C. elegans* DSB-2 protein reveals a regulatory network that controls competence for meiotic DSB formation and promotes crossover assurance. *PLoS Genet.*, **9**, e1003674.
24. Stamper,E.L., Rodenbusch,S.E., Rosu,S., Ahringer,J., Villeneuve,A.M. and Dernburg,A.F. (2013) Identification of DSB-1, a protein required for initiation of meiotic recombination in Caenorhabditis elegans, illuminates a crossover assurance checkpoint. *PLoS Genet.*, **9**, e1003679.
25. Meneely,P.M., McGovern,O.L., Heinis,F.I. and Yanowitz,J.L. (2012) Crossover distribution and frequency are regulated by *him-5* in *Caenorhabditis elegans*. *Genetics*, **190**, 1251–1266.
26. Reddy,K.C. and Villeneuve,A.M. (2004) *C. elegans* HIM-17 links chromatin modification and competence for initiation of meiotic recombination. *Cell*, **118**, 439–452.
27. Kelly,K.O., Dernburg,A.F., Stanfield,G.M. and Villeneuve,A.M. (2000) *Caenorhabditis elegans* msh-5 is required for both normal and radiation-induced meiotic crossing over but not for completion of meiosis. *Genetics*, **156**, 617–630.
28. Zalevsky,J., MacQueen,A.J., Duffy,J.B., Kemphues,K.J. and Villeneuve,A.M. (1999) Crossing over during *Caenorhabditis elegans* meiosis requires a conserved muts-based pathway that is partially dispensable in budding yeast. *Genetics*, **153**, 1271–1283.
29. Yokoo,R., Zawadzki,K.A., Nabeshima,K., Drake,M., Arur,S. and Villeneuve,A.M. (2012) COSA-1 reveals robust homeostasis and separable licensing and reinforcement steps governing meiotic crossovers. *Cell*, **149**, 75–87.
30. Colaiácovo,M.P., MacQueen,A.J., Martinez-Perez,E., McDonald,K., Adamo,A., La Volpe,A. and Villeneuve,A.M. (2003) Synaptonemal complex assembly in *C. elegans* is dispensable for loading strand-exchange proteins but critical for proper completion of recombination. *Dev. Cell*, **5**, 463–474.
31. MacQueen,A.J. (2002) Synapsis-dependent and -independent mechanisms stabilize homolog pairing during meiotic prophase in *C. elegans*. *Genes Dev.*, **16**, 2428–2442.
32. Girard,C., Roelens,B., Zawadzki,K.A. and Villeneuve,A.M. (2018) Interdependent and separable functions of *Caenorhabditiselegans* MRN-C complex members couple formation and repair of meiotic DSBs. *Proc. Natl. Acad. Sci. U.S.A.*, **115**, E4443–E4452.
33. Lemmens,B.B.L.G., Johnson,N.M. and Tijsterman,M. (2013) COM-1 promotes homologous recombination during *Caenorhabditis elegans* meiosis by antagonizing ku-mediated non-homologous end joining. *PLoS Genet.*, **9**, e1003276.
34. Penkner,A., Portik-Dobos,Z., Tang,L., Schnabel,R., Novatchkova,M., Jantsch,V. and Loidl,J. (2007) A conserved function for a *Caenorhabditis elegans* Com1/Sae2/CtIP protein homolog in meiotic recombination. *EMBO J.*, **26**, 5071–5082.
35. Alpi,A., Pasierbek,P., Gartner,A. and Loidl,J. (2003) Genetic and cytological characterization of the recombination protein RAD-51 in *Caenorhabditis elegans*. *Chromosoma*, **112**, 6–16.
36. Dernburg,A.F., McDonald,K., Moulder,G., Barstead,R., Dresser,M. and Villeneuve,A.M. (1998) Meiotic recombination in *C. elegans* initiates by a conserved mechanism and is dispensable for homologous chromosome synapsis. *Cell*, **94**, 387–398.
37. Wagner,C.R., Kuervers,L., Baillie,D.L. and Yanowitz,J.L. (2010) xnd-1 regulates the global recombination landscape in *Caenorhabditis elegans*. *Nature*, **467**, 839–843.
38. Harrell,K., Day,M. and Smolikove,S. (2021) Recruitment of MRE-11 to complex DNA damage is modulated by meiosis-specific chromosome organization. *Mutat. Res.*, **822**, 111743.
39. Hinman,A.W., Yeh,H.-Y., Roelens,B., Yamaya,K., Woglar,A., Bourbon,H.-M.G., Chi,P. and Villeneuve,A.M. (2021) *Caenorhabditis elegans* DSB-3 reveals conservation and divergence among protein complexes promoting meiotic double-strand breaks. *Proc. Natl. Acad. Sci. U.S.A.*, **118**, e2109306118.
40. Caldwell,C.C. and Spies,M. (2020) Dynamic elements of replication protein a at the crossroads of DNA replication, recombination, and repair. *Crit. Rev. Biochem. Mol. Biol.*, **55**, 482–507.
41. Chen,H., Lisby,M. and Symington,L.S. (2013) RPA coordinates DNA end resection and prevents formation of DNA hairpins. *Mol. Cell*, **50**, 589–600.
42. Iyama,T. and Wilson,D.M. (2013) DNA repair mechanisms in dividing and non-dividing cells. *DNA Repair (Amst.)*, **12**, 620–636.

43. Hefel,A., Honda,M., Cronin,N., Harrell,K., Patel,P., Spies,M. and Smolikove,S. (2021) RPA complexes in *Caenorhabditis elegans* meiosis; unique roles in replication, meiotic recombination and apoptosis. *Nucleic Acids Res.*, **49**, 2005–2026.
44. Machovina,T.S., Mainpal,R., Daryabeigi,A., McGovern,O., Paouneskou,D., Labella,S., Zetka,M., Jantsch,V. and Yanowitz,J.L. (2016) A surveillance system ensures crossover formation in *C. elegans*. *Curr. Biol.*, **26**, 2873–2884.
45. Pattabiraman,D., Roelens,B., Woglar,A. and Villeneuve,A.M. (2017) Meiotic recombination modulates the structure and dynamics of the synaptonemal complex during c. elegans meiosis. *PLoS Genet.*, **13**, e1006670.
46. Goodyer,W., Kaitna,S., Couteau,F., Ward,J.D., Boulton,S.J. and Zetka,M. (2008) HTP-3 links DSB formation with homolog pairing and crossing over during *C. elegans* meiosis. *Dev. Cell*, **14**, 263–274.
47. Phillips,C.M., Wong,C., Bhalla,N., Carlton,P.M., Weiser,P., Meneely,P.M. and Dernburg,A.F. (2005) HIM-8 binds to the x chromosome pairing center and mediates chromosome-specific meiotic synapsis. *Cell*, **123**, 1051–1063.
48. Macaisne,N., Kessler,Z. and Yanowitz,J.L. (2018) Meiotic double-strand break proteins influence repair pathway utilization. *Genetics*, **210**, 843–856.
49. Muzzini,D.M., Plevani,P., Boulton,S.J., Cassata,G. and Marini,F. (2008) *Caenorhabditis elegans* POLQ-1 and HEL-308 function in two distinct DNA interstrand cross-link repair pathways. *DNA Repair (Amst.)*, **7**, 941–950.
50. Gagnon,S.N., Hengartner,M.O. and Desnoyers,S. (2002) The genes pme-1 and pme-2 encode two poly(ADP-ribose) polymerases in *Caenorhabditis elegans*. *Biochem. J.*, **368**, 263–271.
51. Amé,J.-C., Fouquerel,E., Gauthier,L.R., Biard,D., Boussin,F.D., Dantzer,F., de Murcia,G. and Schreiber,V. (2009) Radiation-induced mitotic catastrophe in PARG-deficient cells. *J. Cell Sci.*, **122**, 1990–2002.
52. O'Sullivan,J., Tedim Ferreira,M., Gagné,J.-P., Sharma,A.K., Hendzel,M.J., Masson,J.-Y. and Poirier,G.G. (2019) Emerging roles of eraser enzymes in the dynamic control of protein ADP-ribosylation. *Nat. Commun.*, **10**, 1182.
53. Koh,D.W., Lawler,A.M., Poitras,M.F., Sasaki,M., Wattler,S., Nehls,M.C., Stöger,T., Poirier,G.G., Dawson,V.L. and Dawson,T.M. (2004) Failure to degrade poly(ADP-ribose) causes increased sensitivity to cytotoxicity and early embryonic lethality. *Proc. Natl. Acad. Sci. U.S.A.*, **101**, 17699–17704.
54. Menissier de Murcia,J. (2003) Functional interaction between PARP-1 and PARP-2 in chromosome stability and embryonic development in mouse. *EMBO J.*, **22**, 2255–2263.
55. Dantzer,F., Mark,M., Quenet,D., Scherthan,H., Huber,A., Liebe,B., Monaco,L., Chicheportiche,A., Sassone-Corsi,P., de Murcia,G. *et al.* (2006) Poly(ADP-ribose) polymerase-2 contributes to the fidelity of male meiosis i and spermiogenesis. *Proc. Natl. Acad. Sci. U.S.A.*, **103**, 14854–14859.
56. Fong,P.C., Boss,D.S., Yap,T.A., Tutt,A., Wu,P., Mergui-Roelvink,M., Mortimer,P., Swaisland,H., Lau,A., O'Connor,M.J. *et al.* (2009) Inhibition of poly(adp-ribose) polymerase in tumors from *BRCA* mutation carriers. *N. Engl. J. Med.*, **361**, 123–134.
57. Menear,K.A., Adcock,C., Boulter,R., Cockcroft,X., Copsey,L., Cranston,A., Dillon,K.J., Drzewiecki,J., Garman,S., Gomez,S. *et al.* (2008) 4-[3-(4-Cyclopropanecarbonylpiperazine-1-carbonyl)-4-fluorobenzyl]-2 *H* -phthalazin-1-one: a novel bioavailable inhibitor of Poly(ADP-ribose) polymerase-1. *J. Med. Chem.*, **51**, 6581–6591.
58. Robson,M., Im,S.-A., Senkus,E., Xu,B., Domchek,S.M., Masuda,N., Delaloge,S., Li,W., Tung,N., Armstrong,A. *et al.* (2017) Olaparib for metastatic breast cancer in patients with a germline *BRCA* mutation. *N. Engl. J. Med.*, **377**, 523–533.
59. Slade,D. (2020) PARP and PARG inhibitors in cancer treatment. *Genes Dev.*, **34**, 360–394.
60. Raices,M., Bowman,R., Smolikove,S. and Yanowitz,J.L. (2021) Aging negatively impacts DNA repair and bivalent formation in the *C. elegans* germ line. *Front. Cell Dev. Biol.*, **9**, 695333.
61. Loose,J.A., Amrit,F.R.G., Patil,T., Yanowitz,J.L. and Ghazi,A. (2022) Meiotic dysfunction accelerates somatic aging in *Caenorhabditis elegans*. *Aging Cell*, **21**, e13716.
62. Hartman,P.S. and Herman,R.K. (1982) Radiation-sensitive mutants of *Caenorhabditis elegans*. *Genetics*, **102**, 159–178.
63. Bessler,J.B., Andersen,E.C. and Villeneuve,A.M. (2010) Differential localization and independent acquisition of the H3K9me2 and H3K9me3 chromatin modifications in the *Caenorhabditis elegans* adult germ line. *PLoS Genet.*, **6**, e1000830.
64. Fong,Y., Bender,L., Wang,W. and Strome,S. (2002) Regulation of the different chromatin states of autosomes and x chromosomes in the germ line of *C. elegans*. *Science*, **296**, 2235–2238.
65. Gao,J., Kim,H.-M., Elia,A.E., Elledge,S.J. and Colaiácovo,M.P. (2015) NatB domain-containing CRA-1 antagonizes hydrolase ACER-1 linking Acetyl-CoA metabolism to the initiation of recombination during *C. elegans* meiosis. *PLoS Genet.*, **11**, e1005029.
66. Tsai,C.J., Mets,D.G., Albrecht,M.R., Nix,P., Chan,A. and Meyer,B.J. (2008) Meiotic crossover number and distribution are regulated by a dosage compensation protein that resembles a condensin subunit. *Genes Dev.*, **22**, 194–211.
67. Kamp,J.A., van Schendel,R., Dilweg,I.W. and Tijsterman,M. (2020) BRCA1-associated structural variations are a consequence of polymerase theta-mediated end-joining. *Nat. Commun.*, **11**, 3615.
68. Gumienny,T.L., Lambie,E., Hartwieg,E., Horvitz,H.R. and Hengartner,M.O. (1999) Genetic control of programmed cell death in the *Caenorhabditis elegans* hermaphrodite germline. *Development*, **126**, 1011–1022.
69. (1991) More is not better: brood size and population growth in a self-fertilizing nematode. *Proc. R. Soc. Lond. B*, **246**, 19–24.
70. Mortusewicz,O., Fouquerel,E., Amé,J.-C., Leonhardt,H. and Schreiber,V. (2011) PARG is recruited to DNA damage sites through poly(ADP-ribose)- and PCNA-dependent mechanisms. *Nucleic Acids Res.*, **39**, 5045–5056.